Canopy-scale biophysical controls of transpiration and evaporation in the Amazon Basin

Kaniska Mallick[1], Ivonne Trebs[1], Eva Boegh[2], Laura Giustarini[1], Martin Schlerf[1], Darren T. Drewry[3], Lucien Hoffmann[1], Celso von Randow[4], Bart Kruijt[5], Alessandro Araùjo[6], Scott Saleska[7], James R. Ehleringer[8], Tomas F. Domingues[9], Jean Pierre H. B. Ometto[4], Antonio D. Nobre[4], Osvaldo Luiz Leal de Moraes[10], Matthew Hayek[11], J. William Munger[11], Steve Wofsy[11]

[1]Department of Environmental Research and Innovation, Luxembourg Institute of Science and Technology (LIST), Belvaux, Luxembourg

[2]Department of Environmental, Social and Spatial Change, Roskilde University, Roskilde, Denmark

[3]Jet Propulsion Laboratory, California Institute of Technology, 4800 Oak Grove Drive, Pasadena, 91109, USA

[4]Instituto Nacional de Pesquisas Espaciais (INPE), Centro de Ciência do Sistema Terrestre, São José dos Campos, SP, Brazil

[5]Alterra, Wageningen University and Research Centre, Wageningen, The Netherlands

[6]Empresa Brasileira de Pesquisa Agropecuária (EMBRAPA), Belém-PA, Brazil

[7]Department of Ecology and Evolutionary Biology, University of Arizona, Tucson, AZ, USA

[8]Department of Biology, University of Utah, Salt Lake City, UT, USA

[9]Faculdade de Filosofia Ciências e Letras de Ribeirão Preto, Universidade de São Paulo (USP), São Paulo, SP, Brazil

[10]Centro Nacional de Monitoramento e Alertas de Desastres Naturais, SP-RJ, Brazil

[11]Harvard University, Cambridge, MA, USA

Corresponding Authors: Kaniska Mallick (Phone: +352 275888425; Email: kaniska.mallick@gmail.com); Ivonne Trebs **(**Phone: +352 275888880; Email: ivonne.trebs@list.lu**)**

Running head:

Bio-physical controls on evapotranspiration

Abstract:

Canopy and aerodynamic conductances (g_C and g_A) are two of the key land surface biophysical variables that control the land surface response of land surface schemes in climate models. Their representation is crucial for predicting transpiration (λE_T) and evaporation (λE_E) flux components of the terrestrial latent heat flux (λE), which has important implications for global climate change and water resource management. By physical integration of radiometric surface temperature (T_R) into an integrated framework of the Penman-Monteith and Shuttleworth-Wallace model, we present a novel approach to directly quantify the canopy-scale biophysical controls on λE_T and λE_E over multiple plant functional types (PFTs) in the Amazon Basin. Combining data from six LBA (Large-scale Biosphere-Atmosphere Experiment in Amazonia) eddy covariance tower sites and a T_R-driven physically-based modeling approach, we identified the canopy-scale feedback-response mechanism between g_C, λE_T, and atmospheric vapor pressure deficit (D_A), without using any leaf-scale empirical parameterizations for the modelling. The T_R-based model shows minor biophysical control on λE_T during the wet (rainy) seasons where λE_T becomes predominantly radiation driven and net radiation (R_N) determines 75% to 80% of the variances of λE_T. However, biophysical control on λE_T is dramatically increased during the dry seasons, and particularly the 2005 drought year, explaining 50% to 65% of the variances of λE_T and indicates λE_T to be substantially soil moisture driven during rainfall deficit phase. Despite substantial differences in g_A between forests and pastures, very similar canopy-atmosphere 'coupling' was found in these two biomes due to soil moisture induced decrease in g_C in the pasture. This revealed the pragmatic aspect of the T_R-driven model behavior which exhibits a high sensitivity of g_C to per unit change in wetness as opposed to g_A that is not sensitive to surface wetness variability. Our results reveal the occurrence of a significant hysteresis effect between λE_T and g_C during the dry season for the pasture sites, which is

attributed to relatively low soil water availability as compared to the rainforests, likely due to differences in rooting depth between the two systems. Evaporation was significantly influenced by g_A for all the PFTs and across all wetness conditions. Our analytical framework accurately captures the responses of g_C and g_A to changes in radiation forcings, D_A, and surface radiometric temperature, and thus appears to be promising for the improvement of existing land-surface-atmosphere exchange parameterisations across a range of spatial scales.

Keywords: Canopy conductance, aerodynamic conductance, transpiration, evaporation, Penman-Monteith, Shuttleworth-Wallace, coupling, Amazon, LBA

1 Introduction

The Amazon rainforest is one of the world's most extensive natural ecosystems influencing the Earth's water, energy, and carbon cycles (Malhi et al., 2012), and also a major source of global terrestrial evapotranspiration (E) or latent heat flux (λE) (Costa et al., 2010; Harper et al., 2014). An intensification of the Amazon hydrological cycle was observed in the past two decades (Cox et al., 2000; Huntingford et al., 2008; Gloor et al., 2013). Recent Amazonian droughts have gained particular attention due to the sensitivity of the tropical forest λE to climate change (Hilker et al., 2014). If persistent precipitation extremes become more prevalent (Hilker et al., 2014); the Amazon rainforest may increasingly become a net source of carbon as a result of both the suppression of net biome exchange by drought and carbon emissions from fires (Gatti et al., 2014). Changes in land cover due to conversion of tropical forest to pastures significantly alters the energy partitioning of the region by decreasing λE and increasing sensible heat fluxes (H) over pasture sites (e.g. Priante-Filho et al., 2004). This will ultimately lead to severe consequences for the water balance in the region, with modifications to river discharge already observed in some parts of the Basin (Davidson et al., 2012). Evaluating the λE response to changing climate and land use in the Amazon basin is critical to understand the stability of the tropics within the Earth system (Lawrence and Vandecar, 2015). The control of λE can be viewed as complex supply-demand interactions, where net radiation and soil moisture represents the supply and the atmospheric vapor pressure deficit represents the demand. This supply-demand interaction accelerates the biophysical feedbacks in λE and understanding these biophysical feedbacks is necessary to assess the terrestrial biosphere response to water availability. Therefore, quantifying the critical role of biophysical variables on λE will add substantial insight to assessments of the resilience of the Amazon basin under global change.

105 The aerodynamic and canopy conductances (g_A and g_C, hereafter) (unit m s^{-1}) are the two
106 most important biophysical variables regulating the evaporation (λE_E) and transpiration (λE_T)
107 flux components of λE (Monteith and Unsworth, 2008; Dolman et al., 2014; Raupach, 1995;
108 Colaizzi et al., 2012; Bonan et al., 2014). While g_A controls the bulk aerodynamic transfer of
109 energy and water through the near-surface boundary layer, g_C represents the restriction on
110 water vapour flow through the aggregated conductance from stomata of the leaves, in case of
111 a vegetated land surface. In case of partial vegetation cover g_C also includes soil surface
112 conductance for evaporation. At small g_C/g_A ratio, the vapor pressure deficit close to the
113 canopy source/sink height (D_0) approximates the atmospheric vapor pressure deficit (D_A) due
114 to aerodynamic mixing and/or low transpiration. These results in a strong canopy-atmosphere
115 coupling and such conditions are prevalent under soil moisture deficits. On the contrary, large
116 g_C/g_A ratio influences the gradients of vapor pressure deficit just above the canopy, such that
117 D_0 tend towards zero and thus remains different from D_A (Jarvis and McNaughton, 1986).
118 This situation reflects a weak canopy-atmosphere coupling and such situations prevail under
119 predominantly wet conditions and/or poor aerodynamic mixing due to wetness induced low
120 aerodynamic roughness. The Penman-Monteith (PM) equation is a physically-based scheme
121 for quantifying such biophysical controls on canopy-scale λE_E and λE_T from terrestrial
122 ecosystems, treating the vegetation canopy as a 'big-leaf' (Monteith, 1965; 1981). Despite its
123 development based on biophysical principles controlling water vapour exchange, quantifying
124 the g_A and g_C controls on λE through the PM equation suffers from the continued
125 longstanding uncertainty over the aggregated stomatal and aerodynamic behaviour within the
126 soil-plant-atmosphere-continuum (Matheny et al., 2014; Prihodko et al., 2008).

127 One of the major sources of uncertainties in modeling g_A is associated with the empirical (and
128 uncertain) parameterizations of near-surface boundary layer dynamics, which is invariably
129 confounded by space-time variability in atmospheric stability (van der Tol et al., 2009;

Shuttleworth, 1989; Gibson et al., 2011). For example, Monin-Obukhov Similarity Theory (MOST) used for g_A modeling appears to be only valid over uniform, extensive, and flat surfaces (Monteith and Unsworth, 2008; van der Tol et al., 2009; Holwerda et al., 2012), and its application to complex 'real' canopy systems is problematic due to chaotic interactions between turbulence, canopy roughness and topography (Raupach and Finnigan, 1995; Shuttleworth, 2007; Holwerda et al., 2012). Similarly, g_C varies in space and time due to variations in plant species, photosynthetic capacity, soil moisture variability and environmental drivers (Monteith and Unsworth, 2008; van der Tol et al., 2009). Despite the existence of several semi-mechanistic and empirical parameterisations for g_C (e.g. Ball et al., 1987; Leuning, 1995; Tuzet et al., 2003; Medlyn et al., 2011), the adaptive tendencies of plant canopies severely compromises the efficacy of such approaches (Matheny et al., 2014), limiting their applicability over most landscapes. Thus, debate over the most appropriate model of canopy conductance has endured for decades.

Previous studies in the Amazon Basin focused on developing an observational understanding of the biogeochemical cycling of energy, water, carbon, trace gases, and aerosols in Amazonia (Andreae et al., 2002; Malhi et al., 2002; da Rocha et al., 2009), model-based understanding of surface ecophysiological behaviour and seasonality of λE (Baker et al., 2013; Christoffersen et al., 2014), modelling the environmental controls on λE (Hasler and Avissar, 2007; Costa et al., 2010), understanding the seasonality of photosynthesis and of λE (da Rocha et al., 2004; Restrepo-Coupe et al., 2013), and the impact of land use on hydrometeorology (Roy and Avissar, 2002; von Randow et al., 2012). However, the combination of climatic and ecohydrological disturbances will significantly affect stomatal functioning, the partitioning of λE_E-λE_T and carbon-water-climate interactions of tropical vegetation (Cox et al., 2000; Mercado et al., 2009). Hence, investigation of the effects of drought and land cover changes on conductances, λE_E, and λE_T are topics requiring urgent

attention (Blyth et al., 2010) both because of the cursory way it is handled in current generation of parametric models (Matheny et al., 2014) and because of the centrality of g_A and g_C in controlling modelled flux behaviours (Villagarcía et al., 2010). The persistent risk of deforestation is likely to alter the radiation interception, surface temperature, surface moisture, associated meteorological conditions, and vegetation biophysical states of different plant functional types (PFTs). Conversion from forest to pasture is expected to change the g_C/g_A ratio of these ecosystems and impact the evapotranspiration components. Besides inverting the PM equation using field measurements of λE, till date either photosynthesis-dependent modeling or leaf-scale experiments were performed to directly quantify g_C (Ball et al., 1987; Meinzer et al., 1993, 1997; Monteith, 1995; Jones, 1998; Motzer et al., 2005). However, an analytical or physical retrieval for g_A and g_C is required not only to better understand the role of the canopy in regulating evaporation and transpiration, but to enable a capability to characterize the conductances using remote observations, across large spatial domains where in-situ observations are not available. This paper aims to leverage this emerging opportunity by exploring data from the Large-scale Biosphere-Atmosphere Experiment in Amazonia (LBA) eddy covariance (EC) observations (e.g., de Gonçalves et al., 2013; Restrepo-Coupe et al., 2013) using a novel analytical modeling technique, the Surface Temperature Initiated Closure (STIC) (STIC1.0 and STIC1.1) (Mallick et al., 2014, 2015) in order to quantify the biophysical control on λE_E and λE_T over several representative PFTs of the Amazon Basin.

STIC provides a unique framework for simultaneously estimating g_A and g_C, surface energy balance fluxes, λE_E and λE_T. It is based on finding analytical solutions for g_A and g_C by physically integrating radiometric surface temperature (T_R) information (along with radiative fluxes, meteorological variables) into the PM model (Mallick et al., 2014, 2015). The direct estimates of canopy-scale conductances and λE obtained through STIC are independent of

any land surface parameterisation. *This contrasts with the multi-layer canopy models that explicitly parameterize the leaf-scale conductances and perform bottom-up scaling to derive the canopy-scale conductances (Baldocchi et al., 2002; Drewry et al., 2010).* A primary advantage of the approach on which STIC is based is the ability to directly utilize remotely sensed T_R to estimate *E*, thereby providing a capability to estimate *E* over large spatial scales using a remotely sensed variable that is central to many ongoing and upcoming missions. This study presents a detailed examination of the performance of STIC to better understand land-atmosphere interactions in one of the most critical global ecosystems and addresses the following science questions and objectives:

(1) How realistic are canopy-scale conductances when estimated analytically (or non-parametrically) without involving any empirical leaf-scale parameterization?

(2) What are the controls of canopy-scale g_A and g_C on evaporation and transpiration in the Amazon basin, as evaluated using STIC?

(3) How do the STIC-based canopy-scale conductances compare with known environmental constraints?

(4) Is the biophysical response of g_C consistent with the leaf-scale theory (Jarvis and McNaughton, 1986; McNaughton and Jarvis, 1991; Monteith, 1995)?

The following section describes a brief methodology to retrieve g_C, g_A, λE_E, and λE_T. The data sources used for the analysis are described after the methodology and will be followed by a comparison of the results with fluxes derived from EC measurements. A detailed discussion of the results and potential applicability of the method with implications for global change research are elaborated at the end. A list of symbols and variables used in the present study is given in Table 1.

2 Methodology

2.1 Theory

The retrieval of g_A, g_C, and λE are based on finding a 'closure' of the PM equation (eqn. 1 below) using the STIC framework (Fig. A1 in Appendix) (Mallick et al., 2015). STIC is a physically-based single-source surface energy balance scheme which includes internally consistent estimation of g_A and g_C (Mallick et al., 2014, 2015). Originally designed for application to thermal remote sensing data from Earth observation sensors, the STIC framework exploits observations of radiative (T_R), and environmental variables including net radiation (R_N), ground heat flux (G), air temperature (T_A), relative humidity (R_H) or vapor pressure (e_A) at a reference level above the surface.

The foundation of the development of STIC is based on the goal of finding an analytical solution of the two unobserved 'state variables' (g_A and g_C) in the PM equation while exploiting the radiative (R_N and G), meteorological (T_A, R_H), and radiometric surface temperature (T_R) as external inputs. The fundamental assumption in STIC is the first order dependence of g_A and g_C on the aerodynamic temperature (T_0) and soil moisture (through T_R). This assumption allows a direct integration of T_R into the PM equation while simultaneously constraining the conductances through T_R. Although the T_R signal is implicit in R_N, which appears in the numerator of the PM equation (eqn. 1), it may be noted that R_N has a relatively weak dependence on T_R (compared to T_R sensitivities of soil moisture and λE). Given T_R is the direct signature of the soil moisture availability, inclusion of T_R in the PM equation also works to add water stress controls in g_C. Until now the explicit use of T_R in the PM model was hindered due to the unavailability of any direct method to integrate T_R into this model, and, furthermore, due to the lack of physical models expressing biophysical states of vegetation as a function of T_R. Therefore, the majority of the PM-based λE modeling approaches strongly rely on surface reflectance and meteorology while exploiting the

empirical leaf-scale parameterisations of the biophysical conductances (Prihodko et al., 2008; Bonan et al., 2014; Ershadi et al., 2015).

The PM equation is commonly expressed as,

$$\lambda E = \frac{s\phi + \rho c_P g_A D_A}{s + \gamma\left(1 + \frac{g_A}{g_C}\right)} \quad (1)$$

where ρ is the air density (kg m^{-3}), c_P is the specific heat of air (J kg^{-1} K^{-1}), γ is the psychrometric constant (hPa K^{-1}), s is the slope of the saturation vapor pressure versus air temperature (hPa K^{-1}), D_A is the saturation deficit of the air (hPa) or vapor pressure deficit at the reference level, and ϕ is the net available energy (W m^{-2}) (the difference between R_N and G). The units of all the surface fluxes and conductances are in W m^{-2} and m s^{-1}, respectively. For a dense canopy, g_C in the PM equation represents the canopy surface conductance. Although it is not equal to the canopy stomatal conductance, it contains integrated information of the stomata. For a heterogeneous landscape, g_C in the PM equation is an aggregated surface conductance containing information on both canopy and soil. Traditionally, the two unknown 'state variables' in eqn. (1) are g_A and g_C, and the STIC methodology is based on formulating 'state equations' for these conductances that satisfy the PM model (Mallick et al., 2014, 2015). The PM equation is 'closed' upon the availability of canopy-scale measurements of the two unobserved biophysical conductances, and if we assume the empirical models of g_A and g_C to be reliable. However, neither g_A nor g_C can be measured at the canopy-scale or at larger spatial scales. Furthermore, as shown by some recent studies (Matheny et al., 2014; van Dijk et al., 2015), a more appropriate g_A and g_C model is currently not available. This implies that a true 'closure' of the PM equation is only possible through an analytical estimation of the conductances.

2.2 State equations

By integrating T_R with standard surface energy balance (SEB) theory and vegetation biophysical principles, STIC formulates multiple 'state equations' that eliminate the need for exogenous parametric submodels for g_A and g_C, associated aerodynamic variables, and land-atmosphere coupling. The state equations of STIC are as follows and their detailed derivations are described Appendix (A1).

$$g_A = \frac{\phi}{\rho c_P \left[(T_o - T_A) + \left(\frac{e_0 - e_A}{\gamma}\right)\right]} \quad (2)$$

$$g_C = g_A \frac{(e_0 - e_A)}{(e_0^* - e_0)} \quad (3)$$

$$T_o = T_A + \left(\frac{e_0 - e_A}{\gamma}\right)\left(\frac{1 - \Lambda}{\Lambda}\right) \quad (4)$$

$$\Lambda = \frac{2\alpha s}{2s + 2\gamma + \gamma \frac{g_A}{g_C}(1 + M)} \quad (5)$$

Here, T_0 is the temperature (°C) at the source/sink height (or at the roughness length (z_0) or in-canopy air stream), e_0 is the atmospheric vapor pressure (hPa) at the source/sink height, e_0^* is the saturation vapor pressure (hPa) at the source/sink height, Λ is the evaporative fraction (the ratio of λE and ϕ), α is the Priestley-Taylor parameter (unitless) (Priestley and Taylor, 1972), and M is a unitless quantity which describes the relative wetness (or moisture availability) of the surface. M controls the transition from potential to actual evaporation and hence is critical for providing constraint against which the conductances can be estimated (M estimation is explained in Appendix A2). Given values of R_N, G, T_A, and R_H or e_A, the four state equations (eqn. 2 to 5) can be solved simultaneously to derive analytical solutions for the four state variables. This also produces a 'closure' of the PM model, which is independent of empirical parameterizations for both g_A and g_C. However, the analytical solution to the above state equations have four accompanying unknowns; M (surface moisture availability), e_0 (vapor pressure at the source/sink height), e_0^* (saturation vapor pressure at the source/sink

height), and Priestley-Taylor coefficient (α), and as a result there are 4 equations with 8 unknowns. Consequently an iterative solution is needed to determine the four unknown variables (as described in Appendix A2), which is a further modification of the STIC1.1 framework (Mallick et al., 2015). The present version of STIC is designated as STIC1.2 and its uniqueness is the physical integration of T_R into a combined structure of the PM and Shuttleworth-Wallace (SW, hereafter) (Shuttleworth and Wallace, 1985) model to estimate the source/sink height vapor pressures (Appendix A2). In addition to physically integrating T_R observations into a combined PM-SW framework, STIC1.2 also establishes a feedback loop describing the relationship between T_R and λE, coupled with canopy-atmosphere components relating λE to T_0 and e_0. For estimating M, the radiometric surface temperature (T_R) is extensively used in a physical retrieval framework, thus treating T_R as an external input. In eqn. (5), the Priestley-Taylor coefficient (α) appeared due to the use of the Advection-Aridity (AA) hypothesis (Brutsaert and Stricker, 1979) for deriving the state equation of Λ (Supplement S1). However, instead of optimising α as a 'fixed parameter', we have developed a physical equation of α (eqn. A15 in the Appendix A2) and numerically estimated α as a 'variable'. The derivation of the equation for α is described in Appendix A2. The fundamental differences between STIC1.2 and earlier versions are described in Table (A1).

In STIC1.2, T_0 is a function of T_R and they are not assumed equal ($T_0 \neq T_R$). The analytical expression of T_0 is dependent on M and the estimation of M is based on T_R. To further elaborate this point on the inequality of T_0 and T_R, we show an intercomparison of retrieved T_0 versus T_R for forest and pasture (Fig. A2). This indicates the distinct difference of the retrieved T_0 from T_R for the two different biomes.

2.3 Partitioning λE

The terrestrial latent heat flux is an aggregate of both transpiration (λE_T) and evaporation (λE_E) (sum of soil evaporation and interception evaporation from canopy). During rain events the land surface becomes wet and λE tends to approach the potential evaporation (λE^*), while surface drying after rainfall causes λE to approach the potential transpiration rate (λE_T^*) in the presence of vegetation, or zero without any vegetation. Hence, λE at any time is a mixture of these two end member conditions depending on the degree of surface moisture availability or wetness (M) (Bosveld and Bouten, 2003; Loescher et al., 2005). Considering the general case of evaporation from an unsaturated surface at a rate less than the potential, M is the ratio of the actual to the potential evaporation rate and is considered as an index of evaporation efficiency during a given time interval (Boulet et al., 2015). Partitioning of λE into λE_E and λE_T was performed according to Mallick et al. (2014) as follows:

$$\lambda E = \lambda E_E + \lambda E_T = M\lambda E^* + (1-M)\lambda E_T^* \qquad (6)$$

The estimates of λE_E in the current method consists of aggregated contribution from both 'interception' and 'soil evaporation', and no further attempt is made to separate these two components. In the Amazon forest, 'soil evaporation' has a negligible contribution while the 'interception evaporation' contributes substantially to the total evaporative fluxes, and, therefore the partitioning of λE into λE_E and λE_T is crucial. After estimating g_A, λE^* was estimated according to the Penman equation and λE_T was estimated as the residual in eqn. (6).

In this study, we use the term 'canopy conductance' instead of 'stomatal conductance' given the term 'stomata' is applicable at the leaf-scale only. As stated earlier, for a heterogeneous surface g_C should principally be a mixture of the canopy surface (integrated stomatal information) and soil conductances. However, given the high vegetation density of the Amazon Basin, the soil surface exposure is negligible, and, hence we assume g_C to be the

canopy-scale aggregate of the stomatal conductance. Similarly, different g_A exists for soil-canopy, sun-shade, and dry-wet conditions (Leuning, 1995); which is currently integrated into a lumped g_A (given the big-leaf nature of STIC). From the big-leaf perspective, it is generally assumed that the aerodynamic conductance of water vapor and heat are equal (Raupach, 1998). However, for obtaining partitioned aerodynamic conductances, explicit partitioning of λE is needed, which is beyond the scope of the current manuscript.

2.4 Evaluating g_A and g_C

Due to the lack of direct canopy-scale g_A measurements, a rigorous evaluation of g_A cannot be performed. To evaluate the STIC retrievals of g_A ($g_{A\text{-}STIC}$) we adopted three different methods:

(a) By using the measured friction velocity (u^*) and wind speed (u) at the EC towers and using the equation of Baldocchi and Ma (2013) ($g_{A\text{-}BM13}$) in which g_A was expressed as sum of turbulent conductance and canopy (quasi-laminar) boundary layer conductance as,

$$g_{A\text{-}BM13} = [(u/u^{*2}) + (2/ku^{*2})(S_c/P_r)^{0.67}]^{-1} \quad (7)$$

where k is von Karman's constant, 0.4; S_c is the Schmidt Number; P_r is the Prandtl Number and their ratio is generally considered to be unity. Here the conductances of momentum, sensible and latent heat fluxes are assumed to be identical (Raupach, 1998).

(b) By inverting λE observations for wet conditions hence assuming $\lambda E \cong \lambda E^*$ and estimating g_A ($g_{A\text{-}INV}$) as,

$$g_{A\text{-}INV} = \gamma\lambda E/\rho c_P D_A \quad (8)$$

(c) By inverting the aerodynamic equation of H and estimating a hybrid g_A ($g_{A\text{-}HYB}$) from observed H and STIC T_0 as ($T_{0\text{-}STIC}$),

$$g_{A\text{-}HYB} = H/\rho c_P(T_{0\text{-}STIC} - T_A) \quad (9)$$

Like $g_{A\text{-}STIC}$, direct verification of STIC g_C ($g_{C\text{-}STIC}$) could not be performed as canopy-scale g_C observations are not possible with current measurement techniques. Although leaf-scale g_C measurements are relatively straightforward, these values are not comparable to values retrieved at the canopy-scale. However, assuming u^*-based g_A as baseline aerodynamic conductance, we have estimated canopy-scale g_C by inverting the PM equation ($g_{C\text{-}INV}$) (Monteith, 1995) to evaluate $g_{C\text{-}STIC}$ by exploiting $g_{A\text{-}BM13}$ in conjunction with the available ϕ, λE, T_A, and D_A measurements from the EC towers.

2.5 Decoupling coefficient and biophysical controls

The decoupling coefficient or 'Omega' (Ω) is a dimensionless coefficient ranging from 0.0 to 1.0 (Jarvis and McNaughton, 1986) and considered as an index of the degree of stomatal control on transpiration relative to the environment. The equation of Ω is as follows:

$$\Omega = \frac{\frac{s}{\gamma} + 1}{\frac{s}{\gamma} + 1 + \frac{g_A}{g_C}} \tag{10}$$

Introducing Ω in the Penman-Monteith (PM) equation for λE results in:

$$\lambda E = \Omega \lambda E_{eq} + (1 - \Omega)\lambda E_{imp} \tag{11}$$

$$\lambda E_{eq} = \frac{s\phi}{s + \gamma} \tag{12}$$

$$\lambda E_{imp} = \frac{\rho c_P}{\gamma} g_C D_A \tag{13}$$

Where, λE_{eq} is the equilibrium latent heat flux, which depends only on ϕ and would be obtained over an extensive surface of uniform moisture availability (Jarvis and McNaughton, 1986; Kumagai et al., 2004). λE_{imp} is the imposed latent heat flux, which is 'imposed' by the atmosphere on the vegetation surface through the effects of vapor pressure deficit (triggered under limited soil moisture availability) and λE becomes proportional to g_C.

When the g_C/g_A ratio is very small (i.e., water stress conditions), stomata principally control the water loss and a change in g_C will result in a nearly proportional change in transpiration. Such conditions trigger strong biophysical control on transpiration. In this case the Ω value approaches zero and vegetation is believed to be fully coupled to the atmosphere. In contrast, for a high g_C/g_A ratio (i.e., high water availability), changes in g_C will have little effects on the transpiration rate, and transpiration is predominantly controlled by ϕ. In this case the Ω value approaches unity, and vegetation is considered to be poorly coupled to the atmosphere.

Given both g_A and g_C are the independent estimates in STIC1.2, the concept of Ω was used to understand the degree of biophysical control on λE_T, which indicates the extent to which the transpiration fluxes are approaching the equilibrium limit. However, the biophysical characterisation of λE_T and λE_E through STIC1.2 significantly differs from previous approaches (Ma et al., 2015; Chen et al., 2011; Kumagai et al., 2004), and the fundamental differences are centered on the specifications of g_A and g_C (as described in Table A2). While the estimation of g_A in previous approaches is based on u and u^*, the estimation of g_C was based on inversion of observed λE based on the PM equation (e.g. Stella et al., 2013). However, none of these approaches allow independent quantification of biophysical controls of λE as g_C is constrained by λE itself.

3 Datasets

3.1 Eddy covariance and meteorological quantities

We used the LBA (Large-Scale Biosphere-Atmosphere Experiment in Amazonia) data for quantifying the biophysical controls on the evaporative flux components. LBA was an international research initiative conducted from 1995-2005 to study how Amazonia functions as a regional entity within the larger Earth system, and how changes in land use and climate

will affect the hydrological and biogeochemical functioning of the Amazon ecosystem (Andreae et al., 2002).

A network of eddy covariance (EC) towers was operational during the LBA experiment, such that data from nine EC towers were obtained from the ORNL Distributed Archive Active Centre (ftp://daac.ornl.gov/data/lba/carbon_dynamics/CD32_Brazil_Flux_Network/). These are the quality controlled and harmonized surface flux and meteorological data from the Brazilian Amazon flux network. Time series of surface fluxes (λE, H, G), radiation (T_R, R_N, shortwave and longwave), meteorological quantities (T_A, R_H, wind speed) as well as soil moisture and rainfall were available from six (out of nine) EC towers. Three of the EC towers had numerous missing data and were not included in the analysis. The surface energy balance was closed by applying the Bowen ratio (Bowen, 1926) closure as described in Chavez et al. (2005) and later adopted by Anderson et al. (2007) and Mallick et al. (2015). In the absence of G measurements, ϕ was assumed to be equal to the sum of λE and H with the assumption that a dense vegetation canopy restricts the energy incident on the soil surface, thereby allowing us to assume negligible ground heat flux. For the present analysis, data from six selected EC towers (Table 2) represent two different biomes (forest and pasture) covering four different PFTs, namely, tropical rainforest (TRF), tropical moist forest (TMF), tropical dry forest (TDF), and pasture (PAS), respectively. A general description of the datasets can be found in Saleska et al. (2013). For all sites, monthly averages of the diurnal cycle (hourly time resolution) were chosen for the present analysis.

4 Results

4.1 Evaluating g_A, g_C, and surface energy balance fluxes

Examples of monthly averages of the diurnal cycles of the four different g_A estimates and their corresponding g_C estimates over two different PFTs (K34 for forest and FNS for pasture) reveal that $g_{A\text{-}STIC}$ and $g_{C\text{-}STIC}$ tend to be generally higher over the forest than their

counterparts, varying from 0 to 0.06 m s^{-1} and 0 to 0.04 m s^{-1} respectively (Fig. 1a and 1b). The magnitude of $g_{A\text{-}STIC}$ varied between 0 to 0.025 m s^{-1} for the pasture (Fig. 1a), while $g_{C\text{-}STIC}$ values were less than half that of those estimated over the forest (0 – 0.01 m s^{-1}) (Fig. 1b). The conductances showed a marked diurnal variation expressing their overall dependence on net radiation, vapor pressure deficit, and surface temperature. Despite the absolute differences between the conductances from the different retrieval methods, their diurnal patterns were comparable.

The canopy-scale evaluation of $g_{A\text{-}STIC}$ is illustrated in Fig. 2a (and Table 3) combining data from the four PFTs. Estimated values range between zero and 0.1 m s^{-1} and show modest correlation (R^2 = 0.44) (R^2 range between 0.22 [±0.18] to 0.55 [±0.12]) between $g_{A\text{-}BM13}$ and $g_{A\text{-}STIC}$ with regression parameters ranging between 0.81 (±0.023) and 1.07 (±0.047) for the slope and 0.0019 (±0.0006) to 0.0006 (±0.0006) m s^{-1} for the offset (Table 3). The root mean squared deviation (RMSD) varied between 0.007 (TDF) and 0.013 m s^{-1} (TRF). Statistical comparisons between $g_{A\text{-}STIC}$ and $g_{A\text{-}HYB}$ revealed relatively low RMSD and high correlation between them (RMSD = 0.007 m s^{-1} and R^2 = 0.77) as compared to the error statistics between $g_{A\text{-}STIC}$ and $g_{A\text{-}INV}$ (RMSD = 0.011 m s^{-1} and R^2 = 0.50) (Fig. 2b, 2c). The residuals between $g_{A\text{-}STIC}$ and $g_{A\text{-}BM13}$ are plotted as a function of u and u^* in Fig. (2d) with the aim to ascertain whether significant biases are introduced by ignoring wind and shear information within STIC1.2. As illustrated in Fig. 2d, there appears to be a weak systematic relationship between the residual g_A difference with either u^* or u (r = -0.26 and -0.17). However, a considerable relationship was found between wind and shear driven g_A (i.e., $g_{A\text{-}BM13}$) versus ϕ, T_R and D_A (r = 0.83, 0.48, and 0.42) (Fig. 2e and 2f), which indicates that these three energy and water constraints can explain 69%, 23%, and 17% variance of $g_{A\text{-}BM13}$.

Canopy-scale evaluation of hourly g_C is presented in Fig. 3a (and Table 3) combining data from the four PFTs. Estimated values range between zero and 0.06 m s^{-1} for $g_{C\text{-}STIC}$ and show

reasonable correlation (R^2 = 0.39) (R^2 range between 0.14 [±0.04] to 0.58 [±0.12]) between $g_{C\text{-}STIC}$ and $g_{C\text{-}INV}$ with regression parameters ranging between 0.30 (±0.022) and 0.85 (±0.025) for the slope and 0.0024 (±0.0003) to 0.0097 (±0.0007) m s^{-1} for the offset (Table 3). The RMSD varied between 0.007 (PAS) and 0.012 m s^{-1} (TRF and TDF). Given g_A significantly controls g_C, we also examined whether biases in g_C are introduced by ignoring wind and shear information within STIC. The scatterplots between residual g_C difference ($g_{C\text{-}STIC} - g_{C\text{-}INV}$) versus both u and u^* (Fig. 3b) showed g_C residuals to be evenly distributed across the entire range of u and u^* and no systematic pattern was evident.

The reliability of STIC1.2-based g_A and g_C retrievals was further verified by evaluating λE and H estimates (Fig. 4). Both the predicted λE and H are generally in good agreement with the observations, with substantial correlation (r) (R^2 from 0.61 to 0.94), reasonable RMSD of 33 and 37 W m^{-2}, and mean absolute percent deviation (MAPD) of 14% and 32% between the observed and STIC fluxes (Fig. 4). Regression parameters varied between 0.96 (±0.008) to 1.14 (±0.010) for the slope and -16 (±2) to -2 (±2) W m^{-2} for the offset for λE (Table 4), whereas for H, these were 0.60 (±0.025) to 0.89 (±0.035) for the slope and 9 (±1) to 29 (±2) W m^{-2} for the offset (Table 3), respectively. The RMSD in λE varied from 20 to 31 W m^{-2} and 23 to 34 W m^{-2} for H (Table 3).

The evaluation of the conductances and surface energy fluxes indicates some efficacy for the STIC derived fluxes and conductance estimates which represent a weighted average of these variables over the source area around EC tower.

4.2 Canopy coupling, transpiration and evaporation

From Fig. 5a an overall weak to moderate relationship (r = -0.31 to -0.42) is apparent between the coupling (i.e., 1-Ω) and λE_T, where λE_T is negatively related to the coupling for all the PFTs, thus indicating the influence of weak to moderate biophysical controls on λE_T

throughout the year in addition to radiative controls. The biophysical control was substantially enhanced in TRF (r increased from -0.36 to -0.53 and -0.60) (47 to 67% increase) and TMF (r increased from -0.31 to -0.53 and -0.58) (70 to 85% increase) during the dry seasons (July-September) (Fig. 5a). A profound increase of biophysical control on λE_T during the dry season was also found in TDF (52% increase) and PAS (37% increase) (Fig. 5a). The negative relationship (r = -0.29 to -0.45) between (1-Ω) and λE_E (Fig. 5b) in all four PFTs indicated the role of aerodynamic control on λE_E. The aerodynamic control was also enhanced during the dry seasons as shown by the increased negative correlation (r = -0.50 to -0.69) (Fig. 5b) between (1-Ω) and λE_E.

Illustrative examples of the diurnal variations of λE_E, λE_T, and Ω for two different PFTs with different annual rainfall (2329 mm in rainforest, K34 and 1597 mm in pasture, FNS) for three consecutive days during both dry and wet seasons are shown in Fig. 5c to 5f. This shows morning rise of Ω and a near-constant afternoon Ω in the wet season (Fig. 5c and 5d), thus indicating no biophysical controls on λE_E and λE_T during this season. On the contrary, during the dry season, the morning rise in Ω is followed by a decrease during noontime (15% to 25% increase in coupling in forest and pasture) (Fig. 5e and 5f) due to dominant biophysical control, which is further accompanied by a transient increase from mid-afternoon till late afternoon and steadily declined thereafter. Interestingly, coupling was relative higher in pasture during the dry seasons the reasons of which is detailed in the following section and discussion.

4.3 g_C and g_A versus transpiration and evaporation

Scatter plots between λE_T and λE_E versus g_C and g_A showed a triangular pattern which became wider with increasing conductances (Fig. 6). To explain this behaviour of λE_T versus g_C and g_A, we further examined the entire mechanism of conductance-λE_T interactions

475 through two dimensional scatters between λE_T and conductances for two consecutive diurnal
476 cycles during wet and dry seasons over rainforest and pasture sites with different annual
477 rainfall (e.g., K34 as wet and FNS as dry site, annual rainfall 2329 mm and 1597 mm) (Fig.
478 7). Our results confirm the occurrence of diurnal hysteresis between g_C-g_A and λE_T and
479 explain the reason for the shape of the curves obtained in Fig. 6. During the wet season, a
480 distinct environmental control is detectable on g_C and λE_T in the morning hours (Fig. 7a and
481 7b) in both PFTs where g_C and λE_T increased as a result of increasing R_N, T_R, and D_A. From
482 the late morning to afternoon, a near-constant (forest) or negligible increase (pasture) of λE_T
483 is observed despite substantial reduction of both g_C and g_A (25 to 50% decrease), after which
484 λE_T starts decreasing. This behaviour of λE_T was triggered due to the concurrent changes in
485 R_N (15 to 50% change), D_A (20 to 60% change) and surface temperature (T_R) (5% to 14%
486 change), which indicates the absence of any dominant biophysical regulation on λE_T during
487 the wet season (Fig. 7a and 7b). On the contrary in the dry season, although the morning rise
488 in λE_T is steadily controlled by the integrated influence of environmental variables, but a
489 modest to strong biophysical control is found for both PFTs during the afternoon where λE_T
490 substantially decreased with decreasing conductances (Fig. 7c and 7d). This decrease in λE_T
491 is mainly caused by the reduction in g_C as a result of increasing D_A and T_R (as seen later in
492 Fig. 8a and 8c). In the dry season, the area under the hysteretic relationship between λE_T, g_C
493 and environmental variables was substantially wider in pasture (Fig. 7d) than for the
494 rainforest (Fig. 7c), which is attributed to greater hysteresis area between R_N and D_A in
495 pasture as a result of reduced water supply. The stronger hysteresis effects in pasture during
496 the dry season (Fig. 7d) ultimately led to the stronger relationship between coupling and λE_T
497 (as seen in Fig. 5a).

4.4 Factors affecting variability of g_C and g_A

The sensitivity of stomatal conductance to vapor pressure deficit is a key governing factor of transpiration (Ocheltree et al., 2014; Monteith, 1995). We examined if the feedback or feed-forward response hypothesis (Monteith, 1995; Farquhar, 1987) between g_C, D_A, and λE_T is reflected in our canopy-scale g_C retrievals. Combining data of all PFTs, we found an exponential decline of g_C in response to increasing D_A regardless of the variations of net radiation (Fig. 8a). High g_C is consistent with high humidity and low evaporative demand. Five negatively logarithmic scatters fit the data with r values of 0.38 ($0< R_N <150$ W m^{-2}), 0.63 ($150< R_N <300$ W m^{-2}), 0.73 ($300< R_N <450$ W m^{-2}), 0.78 ($450< R_N <600$ W m^{-2}), and 0.87 ($R_N >600$ W m^{-2}). The sensitivity of g_C to D_A was at the maximum in the high R_N range beyond 600 W m^{-2} and the sensitivity progressively declined with declining magnitude of R_N (0 – 150 W m^{-2}).

Scatter plots between g_C and λE_T for different levels of D_A revealed a linear pattern between them for a wide range of D_A ($20> D_A >0$ hPa) (Fig. 8b). Following Monteith (1995), isopleths of R_N are delineated by the solid lines passing through λE_T on the x-axis and through g_C on the y-axis. Isobars of D_A (dotted lines) pass through the origin because λE_T approaches zero as g_C approaches zero. Figure (8b) shows substantial reduction of g_C with increasing D_A without any increase of λE_T, like an inverse hyperbolic pattern to D_A (Monteith 1995; Jones, 1998). For all the PFTs, an active biological (i.e., stomatal) regulation maintained almost constant λE_T when D_A was changed from low to high values (Fig. 8b). At high D_A (above 10 hPa), after an initial increase of λE_T with g_C, g_C approached a maximum limit and remained nearly independent of λE_T (Fig. 8b). Among all the D_A levels, the maximum control of g_C on λE_T variability (62 to 80%) was found at high atmospheric water demand (i.e., 30 hPa>D_A>20 hPa). The scatter plots between g_C and T_R (Fig. 8c) for different levels of D_A revealed an exponential decline in g_C with increasing T_R and atmospheric water demand.

When retrieved g_A was plotted against the radiometric surface temperature and air temperature difference ($T_R - T_A$), an exponential decline in g_A was found in response to increasing ($T_R - T_A$) (Fig. 8d). High g_A is persistent with low ($T_R - T_A$) irrespective of the variations in R_N (with the exception of very low R_N). Four negatively logarithmic scatters fit g_A versus ($T_R - T_A$) relationship with r values of 0.28 ($150< R_N <300$ W m^{-2}), 0.55 ($3000< R_N <450$ W m^{-2}), 0.64 ($450< R_N <600$ W m^{-2}), and 0.77 ($R_N >600$ W m^{-2}).

5 Discussion

5.1 Evaluating g_A, g_C, and surface energy balance fluxes

The aerodynamic conductance retrieved with STIC1.2 showed acceptable correlation and valid estimates of g_A when compared against an empirical model that uses u^* and u to derive g_A (Fig. 1 and 2a) and two other inversion/hybrid-based g_A estimates. The differences between $g_{A\text{-}STIC}$ and $g_{A\text{-}BM13}$ were mainly attributed to the structural differences and empirical nature of the parameterization for the near-surface boundary layer conductance ($(2/ku^{*2})(S_c/P_r)^{0.67}$) in $g_{A\text{-}BM13}$, which results in some discrepancies between $g_{A\text{-}STIC}$ and $g_{A\text{-}BM13}$ particularly in the pasture (Fig. 2a). The extent to which the structural discrepancies between $g_{A\text{-}STIC}$ and $g_{A\text{-}BM13}$ relate to actual differences in the conductances for momentum vs. heat is beyond the scope of this manuscript, and a detailed investigation using data on atmospheric profiles of wind speed, temperature etc. are needed to actually quantify such differences. Momentum transfer is associated with pressure forces and not identical to heat and mass transfer (Massman, 1999). In STIC1.2, g_A is directly estimated and is a robust representative of the conductances to heat/water vapor transfer; whereas $g_{A\text{-}BM13}$ estimates based on u^* and u is more representative for the momentum transfer. Therefore, the difference between the two different g_A estimates (Fig. 2) can be largely attributed to the actual difference in the conductances for momentum and heat/water vapor. The turbulent conductance equation (u^{*2}/u) in $g_{A\text{-}BM13}$ is also very sensitive to the uncertainties in the sonic anemometer

548 measurement (Contini et al., 2006; Richiardone et al., 2012). However, the evidence of a
549 weak systematic relationship between the g_A residuals and u (Fig. 2d) and capability of the
550 thermal (T_R), radiative (ϕ), and meteorological (T_A, D_A) variables in capturing the variability
551 of $g_{A\text{-}BM13}$ (Fig. 2e and 2f) indicates the diagnostic potential $g_{A\text{-}STIC}$ estimates to explain the
552 wind driven g_A variability. Excluding u might introduce errors in cases where wind is the
553 only source of variations in g_A and surface fluxes (Mallick et al., 2015). In general, the
554 accuracies in commonly used parametric g_A estimates based on u and surface roughness
555 parameters several meters distant from canopy foliage is limited due to the uncertainties
556 concerning the attenuation of u close to the vegetation surface (Meinzer et al., 1997; Prihodko
557 et al., 2008). The magnitude of u near the foliage can be substantially lower than that
558 measured considerably away at some reference location above or within the canopy (Meinzer
559 et al., 1997). Notwithstanding the inequalities of g_A estimated with different methods, it is
560 challenging to infer the accuracy of the different estimates. It is imperative to mention that g_A
561 is one of the main anchors in the PM-SW model because it not only appears in the numerator
562 and denominator of these models, g_A also provides feedback to g_C, T_0, and D_0 (seminal paper
563 of Jarvis and McNaughton, 1986). Therefore, the estimates of λE in the PM-SW framework
564 are very sensitive to parameterization of g_A and stable λE estimates might be possible if g_A
565 estimation is unambiguous (Holwerda et al., 2012; van Dijk et al., 2015). Given the lack of
566 consensus in the community on the 'true' g_A and from the nature of surface flux validation
567 results (Fig. 4) it appears that $g_{A\text{-}STIC}$ tends to be the appropriate aerodynamic conductance
568 that satisfies the PM-SW equation. Discrepancies between $g_{C\text{-}STIC}$ and $g_{C\text{-}INV}$ originated from
569 the differences in g_A estimates between the two methods.

570 Despite the good agreement between the measured and predicted λE and H (Fig. 4, Table 4),
571 the larger error in H was associated with the higher sensitivity of H to the errors in T_R (due to
572 poor emissivity correction) (Mallick et al., 2015). Since the difference between T_R and T_A is

considered to be the primary driving force of H (van der Tol et al., 2009), the modelled errors in H are expected to arise due to the uncertainties associated with T_R.

5.2 Canopy coupling, g_C and g_A versus transpiration and evaporation

The correlation analysis between 1-Ω and λE_T revealed the extent of biophysical and radiative controls on λE_T (Fig. 5). The degree of biophysical control is a function of the ratio of g_C to g_A. Minor biophysical control on λE_T was apparent for forest and pasture during the wet seasons (Fig. 5c and 5d) as a result of a high g_C/g_A ratio along with increasing λE_T. Such conditions stimulate local humidification of air surrounding the canopy and uncoupling of the in-canopy vapor pressure deficit (D_0) from that in the air above (i.e., $D_0<D_A$) (Meinzer et al., 1997; Motzer et al., 2005) (Fig. 9a), which implies that λE_T becomes largely independent of g_C. On the contrary, an enhanced biophysical control on λE_T was apparent during the dry season and drought year 2005 during the period of reduced water supply particularly over PAS (Fig. 5e, 5f, and 7). Such condition leads to a relatively dry canopy surface, and substantially high g_A compared to g_C, thus resulting in low g_C/g_A ratios regardless of their absolute values (Meinzer et al., 1993; McNaughton and Jarvis, 1991). Here, fractional changes in g_C results in an equivalent fractional change in λE_T. This impedes transpiration from promoting local equilibrium of D_0 and minimizing (or maximizing) the gradient between D_0 and atmospheric vapor pressure deficit (D_A) (i.e., $D_0 \cong D_A$ or $D_0>D_A$) (eqn. A10) (Fig 9a), thereby resulting in strong coupling between D_0 and D_A (Meinzer et al., 1993; Jarvis and McNaughton, 1986). Besides, a supplemental biophysical control on λE_T might have been imposed as a consequence of a direct negative feedback of D_A and D_0 on g_C (McNaughton and Jarvis, 1991; Jarvis, 1986). Increase in D_A (or D_0) beyond a certain limit decreases g_C (Fig. 7 and 8), resulting in a low and narrow increase of λE_T, despite steady increase in g_A and R_N. The combination of negative feedback response between D_A and g_C

with the overall radiative-aerodynamic coupling significantly dampens the variation of transpiration in PAS and TDF in the dry season, thus featuring increased biophysical control in these PFTs. These results are in agreement with von Randow et al. (2012), who found enhanced biophysical control on λE_T for the pasture during the dry season. For the wet season, evidence of minor biophysical control indicates the dominance of R_N driven equilibrium evaporation in these PFTs (Hasler and Avissar, 2007; da Rocha et al., 2009; Costa et al., 2010). In the TRF and TMF, 94% and 99% of the retrieved g_C/g_A ratios fall above 0.5, and, only 1% and 6% of the retrieved g_C/g_A ratios fall below the 0.5 range (Fig. 9b). In contrast, 90% and 73% of the g_C/g_A ratios range above 0.5, and 10% to 27% of the g_C/g_A ratios were below 0.5 for TDF and PAS, respectively (Fig. 9b). This shows that, although radiation control is prevailing in all the sites, biophysical control is relatively stronger in TDF and PAS as compared to the other sites. For large g_C/g_A ratios, the conditions within the planetary boundary layer (PBL) become decoupled from the synoptic scale (McNaughton and Jarvis, 1991) and the net radiative energy becomes the important regulator of transpiration. For small g_C/g_A ratios (e.g., in dry season), the conditions within the PBL are strongly coupled to the atmosphere above by rapid entrainment of air from the capping inversion and by some ancillary effects of sensible heat flux on the entrainment (McNaughton and Jarvis, 1991). These findings substantiate the earlier theory of McNaughton and Jarvis (1991), who postulated that large g_C/g_A ratios result in minor biophysical control on canopy transpiration due to the negative feedback on the canopy from the PBL. The negative relationship between 1-Ω and λE_E (Fig. 5b) over all the PFTs is due to the feedback of g_A on g_C. However, over all the PFTs, a combined control of g_A and environmental variables on λE_E again highlighted the impact of realistically estimated g_A on λE_E (Holwerda et al., 2012).

It is important to mention that forests are generally expected to be better coupled to the atmosphere, which is related to generally higher g_A (due to high surface roughness) compared to the pastures. This implies that forests exhibit stronger biophysical control on λE_T. However, due to the broad leaves of the rain forests (larger leaf area index) and higher surface wetness (due to higher rainfall amounts) the wet surface area is much larger in the forest than in the pastures. This results in much higher g_C values for forests than for pastures during the wet season ($g_C \approx g_A$), and $g_C/g_A \rightarrow 1$. Consequently, no significant difference in coupling was found between them during the wet season (Fig. 5c and 5d). Despite the absolute differences in g_A and g_C between forest and pasture, the high surface wetness is largely offsetting the expected Ω difference between them. Although the surface wetness is substantially lower during the dry season, the high water availability in the forests due to the deeper root systems help maintaining a relatively high g_C compared to the pastures. Hence, despite g_A (forest) > g_A (pasture) during the dry season, substantially lower g_C values for the pasture result in lower g_C/g_A ratio for the pasture compared to the forest, thus causing more biophysical control on λE_T during the dry season. The relatively better relationship between coupling versus λE_T in PAS and TDF during the dry season was also attributed to high surface air temperature difference ($T_R - T_A$) in these PFTs that resulted in low g_C/g_A ratios (Fig. 9c).

5.3 Factors affecting g_C and g_A variability

The stomatal feedback-response hypothesis (Monteith, 1995) also became apparent at the canopy-scale (Fig. 8a, 8b), which states that a decrease in g_C with increasing D_A is caused by a direct increase in λE_T (Monteith, 1995; Matzner & Comstock, 2001; Streck, 2003) and g_C responds to the changes in the air humidity by sensing λE_T, rather than D_A. This feedback mechanism is found because of the influence of D_A on both g_C and λE_T, which in turn changes D_A by influencing the air humidity (Monteith, 1995). The change in g_C is dominated

by an increase in the net available energy, which is partially offset by an increase in λE_T. After the net energy input in the canopy exceeds a certain threshold, g_C starts decreasing even if λE_T increases. High λE_T increases the water potential gradient between guard cells and other epidermal cells or reduces the bulk leaf water potential, thus causing stomatal closure (Monteith, 1995; Jones, 1998; Streck, 2003). The control of soil water on transpiration also became evident from the scatter plots between g_C versus λE_T and T_R for different D_A levels (Fig. 8b, 8c) (also Fig. 7). Denmead and Shaw (1962) hypothesized that reduced g_C and stomatal closure occurs at moderate to higher levels of soil moisture (high λE_T) when the atmospheric demand of water vapor increases (high D_A). The water content in the immediate vicinity of the plant root depletes rapidly at high D_A, which decreases the hydraulic conductivity of soil, and the soil is unable to efficiently supply water under these conditions. For a given evaporative demand and available energy, transpiration is determined by the g_C/g_A ratio, which is further modulated by the soil water availability. These combined effects tend to strengthen the biophysical control on transpiration (Leuzinger and Kirner, 2010; Migletta et al., 2011). The complex interaction between g_C, T_R, and D_A (Fig. 8c) explains why different parametric g_C models produce divergent results.

Although λE_T and λE_E estimates are interdependent on g_C and g_A (as shown in Fig. 6 to Fig. 8); the figures reflect the credibility of the conductances as well as transpiration estimates by realistically capturing the hysteretic behavior between biophysical conductances and water vapor fluxes, which is frequently observed in natural ecosystems (Zhang et al., 2014, Renner et al., 2016). These results are also compliant with the theories postulated earlier from observations that the magnitude of hysteresis depends on the radiation-vapor pressure deficit time-lag, while the soil moisture availability is a key factor modulating the hysteretic transpiration-vapor pressure deficit relation as soil moisture declines (Zhang et al., 2014; O'Grady et al., 1999; Jarvis and McNaughton, 1986). This shows that despite being

independent of any predefined hysteretic function, the interdependent conductance-transpiration hysteresis is still captured in STIC1.2.

Fig. 8d is in accordance with existing theory that under conditions of extremely high atmospheric turbulence (i.e., high g_A), a close coupling exists between the surface and the atmosphere, which causes T_R and T_A to converge (i.e., $T_R - T_A \rightarrow 0$). When g_A is low, the difference between T_R and T_A increases due to poor vertical mixing of the air.

6 Conclusions

By integrating the radiometric surface temperature (T_R) into a combined structure of PM-SW model we have estimated the canopy-scale biophysical conductances and quantified their control on the terrestrial evapotranspiration components in a simplified SEB modeling perspective that treats the vegetation canopy as 'big-leaf'. The STIC1.2 biophysical modeling scheme is independent of any leaf-scale empirical parameterisation for stomata and associated aerodynamic variables.

Stomata regulate the coupling between terrestrial carbon and water cycles, which implies that their behaviour under global environmental change is critical to predict vegetation functioning (Medlyn et al., 2011). The combination of variability in precipitation (Hilker et al., 2014) and land cover change (Davidson et al., 2012) in the Amazon Basin is expected to increase the canopy-atmosphere coupling of pasture or forest systems under drier conditions by altering the ratio of the biological and aerodynamic conductances. An increase of biophysical control will most likely be an indicator of shifting the transpiration from an energy-limited to a water-limited regime (due to the impact of T_R, T_A, and D_A on the g_C/g_A ratio) with further consequences for the surface water balance and rainfall recycling. At the same time, a transition from forest to pasture or agriculture lands will substantially reduce the contribution of interception evaporation in the Amazon, hence, it will affect the regional water cycle. This might change the moisture regime of the Amazonian Basin and affect the

moisture transport to other regions. In this context, STIC1.2 provides a new quantitative and internally consistent method for interpreting the biophysical conductances and able to quantify their controls on the water cycle components in response to a range of climatic and ecohydrological conditions (excluding rising atmospheric CO_2) across a broad spectrum of PFTs. It could also provide the basis to improve existing land surface parameterisations for simulating vegetation water use at large spatial scales.

It should also be noted that although the case study described here provides general insights into the biophysical controls of λE and associated feedback between g_C, D_A, T_R and λE_T in the framework of the PM-SW equation, there is a tendency for overestimation of g_C due to the embedded evaporation information in the current single-source composition of STIC1.2. For accurate characterisation of canopy conductance, explicit partitioning of λE into transpiration and evaporation (both soil and interception) is one of the further scopes for improving STIC1.2 and this assumption needs to be tested further.

Acknowledgements

The developed modeling framework contributes to the "Catchments As Organized Systems (CAOS)" Phase-2 research group (FOR 1598) funded by the German Science Foundation (DFG) and to the "HiWET (High-resolution modelling and monitoring of Water and Energy Transfers in wetland ecosystems)" consortium funded by BELSPO and FNR. We sincerely thank Dr. Andrew Jarvis (Lancaster University, UK), Dr. Monica Garcia (Technical University of Denmark, Denmark), and Dr. Georg Wohlfahrt (University of Innsbruck, Austria) for very helpful discussions and edits in the manuscript. We are grateful to all Brazilian and international collaborators and all the funding agencies that have contributed to the Large-scale Biosphere Atmosphere Experiment in Amazônia (LBA). The authors are indebted to Pavel Kabat, Antônio Ocimar Manzi, David R. Fitzjarrald, Julio Tota, Humberto Ribeiro da Rocha, Michael Goulden, Maarten J. Waterloo and Luiz Martinelli for planning,

coordinating, conducting, and evaluating the eddy covariance, meteorological and leaf gas exchange measurements at the LBA sites. We are particularly grateful to all field technicians whose hard work were the key ingredients to establish the quality of the datasets used in this paper. The authors declare no conflict of interest. DTD acknowledges support of the Jet Propulsion Laboratory, California Institute of Technology, under a contract with the National Aeronautics and Space Administration.

Appendix A:

A1 Derivation of 'state equations' in STIC 1.2

Neglecting horizontal advection and energy storage, the surface energy balance equation is written as follows:

$$\phi = \lambda E + H \tag{A1}$$

Figure (A1) shows that, while H is controlled by a single aerodynamic resistance (r_A) (or $1/g_A$); λE is controlled by two resistances in series, the surface resistance (r_C) (or $1/g_C$) and the aerodynamic resistance to vapor transfer ($r_C + r_A$). For simplicity, it is implicitly assumed that the aerodynamic resistance of water vapor and heat are equal (Raupach, 1998), and both the fluxes are transported from the same level from near surface to the atmosphere. The sensible and latent heat flux can be expressed in the form of aerodynamic transfer equations (Boegh et al., 2002; Boegh and Soegaard, 2004) as follows:

$$H = \rho c_P g_A (T_o - T_A) \tag{A2}$$

$$\lambda E = \frac{\rho c_P}{\gamma} g_A (e_0 - e_A) = \frac{\rho c_P}{\gamma} g_C (e_0^* - e_0) \tag{A3}$$

Where T_0 and e_0 are the air temperature and vapor pressure at the source/sink height (i.e., aerodynamic temperature and vapor pressure) or at the so-called roughness length (z_0), where wind speed is zero. They represent the vapor pressure and temperature of the quasi-laminar boundary layer in the immediate vicinity of the surface level (Fig. A1), and T_0 can be

obtained by extrapolating the logarithmic profile of T_A down to z_0. e_0^* is the saturation vapor pressure at T_0 (hPa).

By combining eqn. (A1), (A2), and (A3) and solving for g_A, we get the following equation.

$$g_A = \frac{\phi}{\rho c_P \left[(T_o - T_A) + \left(\frac{e_0 - e_A}{\gamma}\right)\right]} \tag{A4}$$

Combining the aerodynamic expressions of λE in eqn. (A3) and solving for g_C, we can express g_C in terms of g_A, e_0^*, e_0, and e_A.

$$g_C = g_A \frac{(e_0 - e_A)}{(e_0^* - e_0)} \tag{A5}$$

While deriving the expressions for g_A and g_C, two more unknown variables are introduced (e_0 and T_0), thus there are two equations and four unknowns. Therefore, two more equations are needed to close the system of equations.

An expression for T_0 is derived from the Bowen ratio (β) (Bowen, 1926) and evaporative fraction (Λ) (Shuttleworth et al., 1989) equation.

$$\beta = \left(\frac{1 - \Lambda}{\Lambda}\right) = \frac{\gamma(T_0 - T_A)}{(e_0 - e_A)} \tag{A6}$$

$$T_o = T_A + \left(\frac{e_0 - e_A}{\gamma}\right)\left(\frac{1 - \Lambda}{\Lambda}\right) \tag{A7}$$

This expression for T_0 introduces another new variable (Λ); therefore, one more equation that describes the dependence of Λ on the conductances (g_A and g_C) is needed to close the system of equations. In order to express Λ in terms of g_A and g_C, we had adopted the advection – aridity (AA) hypothesis (Brutsaert and Stricker, 1979) with a modification introduced by (Mallick et al., 2015). The AA hypothesis is based on a complementary connection between the potential evaporation (E^*), sensible heat flux (H), and E; and leads to an assumed link between g_A and T_0. However, the effects of surface moisture (or water stress) were not explicit in the AA equation and Mallick et al. (2015) implemented a moisture constraint in the original advection-aridity hypothesis while deriving a 'state equation' of Λ (eqn. A8

761 below). A detailed derivation of the 'state equation' for Λ is described in the Supplement (S1)
762 (also see Mallick et al., 2014, 2015). Estimation of e_0, e_0^*, M, and α is described in the
763 Appendix (A2).

$$\Lambda = \frac{2\alpha s}{2s + 2\gamma + \gamma \frac{g_A}{g_C}(1+M)} \quad \text{(A8)}$$

764 **A2 Iterative solution of e_0, e_0^*, M, and α in STIC 1.2**

765 In STIC1.0 and 1.1 (Mallick et al., 2014; 2015), no distinction was made between the surface
766 and source/sink height vapor pressures. Therefore, e_0^* was approximated as the saturation
767 vapor pressure at T_R and e_0 was empirically estimated from M based on the assumption that
768 the vapor pressure at the source/sink height ranges between extreme wet–dry surface
769 conditions. However, the level of e_0 and e_0^* should be consistent with the level of the
770 aerodynamic temperature (T_0) from which the sensible heat flux is transferred (Lhomme and
771 Montes, 2014). The predictive use of the PM model could be hindered due to neglecting the
772 feedbacks between the surface layer evaporative fluxes and source/sink height mixing and
773 coupling (McNaughton and Jarvis, 1984), and their impact on the canopy scale conductances.
774 Therefore, in STIC1.2, we have used physical expressions for estimating e_0 and e_0^* followed
775 by estimating T_{SD} and M as described below. The fundamental differences between STIC1.0,
776 1.1 and 1.2 modeling philosophy is described in Table A1.

777 An estimate of e_0^* is obtained by inverting the aerodynamic transfer equation of λE.

$$e_0^* = e_A + \left[\frac{\gamma \lambda E (g_A + g_C)}{\rho c_P g_A g_C}\right] \quad \text{(A9)}$$

778 Following Shuttleworth and Wallace (1985) (SW85), the vapor pressure deficit (D_0) (= e_0^* -
779 e_0) and vapor pressure (e_0) at the source/sink height are expressed as follows.

$$D_0 = D_A + \left[\frac{\{s\phi - (s + \gamma)\lambda E\}}{\rho c_P g_A}\right] \quad \text{(A10)}$$

$$e_0 = e_0^* - D_0 \quad \text{(A11)}$$

780 A physical equation of α is derived by expressing the evaporative fraction (Λ) as function of
781 the aerodynamic equations of H $[\rho c_P g_A(T_0 - T_A)]$ and λE $[\frac{\rho c_P}{\gamma}\frac{g_A g_C}{g_A+g_C}(e_0^* - e_A)]$ as follows.

$$\Lambda = \frac{\lambda E}{H + \lambda E} \quad \text{(A12)}$$

$$= \frac{\frac{\rho c_P}{\gamma}\frac{g_A g_C}{g_A + g_C}(e_0^* - e_A)}{\rho c_P g_A(T_0 - T_A) + \frac{\rho c_P}{\gamma}\frac{g_A g_C}{g_A + g_C}(e_0^* - e_A)} \quad \text{(A13)}$$

$$= \frac{g_C(e_0^* - e_A)}{[\gamma(T_0 - T_A)(g_A + g_C) + g_C(e_0^* - e_A)]} \quad \text{(A14)}$$

782 Combining eqn. (A14) and eqn. (A8) (eliminating Λ), we can derive a physical equation of α.

$$\alpha = \frac{g_C(e_0^* - e_A)\left[2s + 2\gamma + \gamma\frac{g_A}{g_C}(1 + M)\right]}{2s[\gamma(T_0 - T_A)(g_A + g_C) + g_C(e_0^* - e_A)]} \quad \text{(A15)}$$

783 Following Venturini et al. (2008), M can be expressed as the ratio of the vapor pressure
784 difference to the vapor press deficit between surface to atmosphere as follows.

$$M = \frac{(e_0 - e_A)}{(e_0^* - e_A)} = \frac{(e_0 - e_A)}{\kappa(e_S^* - e_A)} = \frac{s_1(T_{SD} - T_D)}{\kappa s_2(T_R - T_D)} \quad \text{(A16)}$$

785 Where T_{SD} is the dewpoint temperature at source/sink height and T_D is the air dewpoint
786 temperature; s_1 and s_2 are the psychrometric slopes of the saturation vapor pressure and
787 temperature between ($T_{SD} - T_D$) versus ($e_0 - e_A$) and ($T_R - T_D$) versus (e_s^* - e_A) relationship
788 (Venturini et al., 2008); and κ is the ratio between (e_0^* - e_A) and (e_s^* - e_A). Despite T_0 drives
789 the sensible heat flux, the comprehensive dry-wet signature of underlying surface due to soil
790 moisture variations is directly reflected in T_R (Kustas and Anderson, 2009). Therefore, using

791 T_R in the denominator of eqn. (A16) tend to give a direct signature of the surface moisture
792 availability (M). In eqn. (A16), T_{SD} computation is challenging because both e_0 and s_1 are
793 unknown. By decomposing the aerodynamic equation of λE, T_{SD} can be expressed as follows.

$$\lambda E = \frac{\rho c_P}{\gamma} g_A (e_0 - e_A) = \frac{\rho c_P}{\gamma} g_A s_1 (T_{SD} - T_D)$$

$$T_{SD} = T_D + \frac{\gamma \lambda E}{\rho c_P g_A s_1} \quad \text{(A17)}$$

794 In the earlier STIC versions, s_1 was approximated at T_D, e_0^* was approximated at T_R, T_{SD} was
795 estimated from s_1, T_D, T_R, and related saturation vapor pressures (Mallick et al., 2014; 2015),
796 and M was estimated from eqn. (A16) (estimation of T_{SD} and M was stand-alone earlier).
797 However, since T_{SD} depends on λE and g_A, an iterative procedure is applied to estimate T_{SD}
798 and M as described below.

799 In STIC1.2, an initial value of α is assigned as 1.26 and initial estimates of e_0^* and e_0 are
800 obtained from T_R and M as $e_0^* = 6.13753 e^{\frac{17.27 T_R}{(T_R + 237.3)}}$ and $e_0 = e_A + M(e_0^* - e_A)$. Initial T_{SD}
801 and M were estimated as described above. With the initial estimates of these variables; first
802 estimate of the conductances, T_0, Λ, and λE are obtained. The process is then iterated by
803 updating e_0^* (using eqn. A9), D_0 (using eqn. A10), e_0 (using eqn. A11), T_{SD} (using eqn. A17
804 with s_1 estimated at T_D), M (using eqn. A16), and α (using eqn. A15), with the first estimates
805 of g_C, g_A, and λE, and recomputing g_C, g_A, T_0, Λ, and λE in the subsequent iterations with the
806 previous estimates of e_0^*, e_0, T_{SD}, M, and α until the convergence λE is achieved. Stable
807 values of λE, e_0^*, e_0, T_{SD}, M, and α are obtained within ~25 iterations. Illustrative examples
808 of the convergence of e_0^*, e_0, T_{SD}, M, and α are shown in Fig. (A3).

809 To summarize, the computational steps of the conductances and evaporative fluxes in STIC
810 are:

Step 1: Analytical solution of the conductances, T_0 and Λ by solving the 'state equations' (eqn. 2, 3, 4, and 5). Step 2: Initial estimates of the conductances (g_C and g_A), T_0, Λ, λE and H. Step 3: Simultaneous iteration of λE, e_0^*, e_0, T_{SD}, M, and α*; and final estimation of the conductances (g_C and g_A), T_0, Λ, λE and H. Step 4: Partitioning λE intoλE_T and λE_E.*

832

833

834 **References:**

835 Andreae, M.O., Artaxo, P., Brandao, C., et al.: Biogeochemical cycling of carbon, water,
836 energy, trace gases, and aerosols in Amazonia: The LBA-EUSTACH experiments, J.
837 Geophys. Res., 107, D20, 8066, doi:10.1029/2001JD000524, 2002.

838 Baker, I.T., Harper, A.B., da Rocha, H.R., Denning, A.S., et al.: Surface ecophysiological
839 behavior across vegetation and moisture gradients in tropical South America, Agric. For.
840 Meteorol., 182– 183, 177– 188, 2013.

841 Baldocchi, D.D., Wilson, K., and Gu, L.: How the environment, canopy structure and canopy
842 physiological functioning influence carbon, water and energy fluxes of a temperate
843 broad-leaved deciduous forest-An assessment with the biophysical model CANOAK,
844 Tree Phys., 22(15–16), 1065, 2002.

845 Baldocchi, D.D., and Ma, S.: How will land use affect air temperature in the surface
846 boundary layer? Lessons learned from a comparative study on the energy balance of an
847 oak savanna and annual grassland in California, USA, Tellus B, 65, 19994,
848 http://dx.doi.org/10.3402/tellusb.v65i0.19994, 2013.

849 Ball, J.T., Woodrow, I.E., and Berry, J.A.: A model predicting stomatal conductance and its
850 contribution to the control of photosynthesis under different environmental conditions.
851 *In: Progress in Photosynthesis Research*, ed. J Biggins. M Nijhoff, Dordrecht, *4*, 5.221-
852 5.224, Martinus-Nijhoff Publishers, Dordrecht, The Netherlands, 1987.

853 Blyth, E., Gash, J., Lloyd, A., Pryor, M., Weedon, G.P., and Shuttleworth, W.J.: Evaluating
854 the JULES Land Surface Model Energy Fluxes Using FLUXNET Data, J.
855 Hydrometeorol., 11, 509–519, doi: http://dx.doi.org/10.1175/2009JHM1183.1, 2010.

Boegh, E., Soegaard, H., and Thomsen, A.: Evaluating evapotranspiration rates and surface conditions using Landsat TM to estimate atmospheric resistance and surface resistance, Remote Sens. Environ., 79, 329 – 343, 2002.

Boegh, E., and Soegaard, H.: Remote sensing based estimation of evapotranspiration rates, Int. J. Remote Sens., 25 (13), 2535 – 2551, 2004.

Bonan, G.B., Williams, M., Fisher, R.A., and Oleson, K.W.: Modeling stomatal conductance in the earth system: linking leaf water-use efficiency and water transport along the soil–plant–atmosphere continuum, Geosci. Model Development, 7, 2193–2222, doi:10.5194/gmd-7-2193-2014, 2014.

Bosveld, F.C., and Bouten, W.: Evaluating a model of evaporation and transpiration with observations in a partially wet Douglas-fir forest, Boundary Layer Meteorol., 108, 365 – 396, 2003.

Boulet, G., Mougenot, B., Lhomme, J.-P., Fanise, P., et al.: The SPARSE model for the prediction of water stress and evapotranspiration components from thermal infra-red data and its evaluation over irrigated and rainfed wheat, Hydrol. Earth Syst. Sci., 19, 4653-4672, doi:10.5194/hess-19-4653-2015, 2015.

Bowen, I. S.: The ratio of heat losses by conduction and by evaporation from any water surface, Physics Rev., 27, 779–787, 1926.

Brutsaert, W., and Stricker, H.: An advection-aridity approach to estimate actual regional evapotranspiration, Water Resour. Res., 15 (2), 443– 450, 1979.

Chen, L., Zhang, Z., Li, Z., Tang, J., et al.: Biophysical control of whole tree transpiration under an urban environment in Northern China, J. Hydrol., 402, 388 – 400, 2011.

Chen, F., and Schwerdtfeger, P.: Flux-gradient relationships for momentum and heat over a rough natural surface. Quar. J. Royal Met. Soc., 115, 335-352, 1989.

880 Choudhury, B. J., and Monteith, J. L.: Implications of stomatal response to saturation deficit
881 for the heat balance of vegetation, Agric. For. Meteorol., 36, 215 – 225, 1986.
882 Christoffersen, B.O., Restrepo-Coupe, N., Arain, M.A., and Baker, I.T., et al.: Mechanisms of
883 water supply and vegetation demand govern the seasonality and magnitude of
884 evapotranspiration in Amazonia and Cerrado, Agric. For. Meteorol., 191, 33 – 50, 2014.
885 Colaizzi, P.D., Kustas, W.P., and Anderson, M.C., et al.: Two-source energy balance model
886 estimates of evapotranspiration using component and composite surface temperatures,
887 Adv. Water Resour., 50, 134-151, 2012.
888 Contini, D., Donateo, A., and Belosi, F.: Accuracy of Measurements of Turbulent Phenomena
889 in the Surface Layer with an Ultrasonic Anemometer, J. Atm. Oceanic Tech., 23, 785–
890 801, doi: http://dx.doi.org/10.1175/JTECH1881.1, 2006.
891 Costa, M.H., Biajoli, M.C., Sanches, L., Malhado, A.C.M. et al. : Atmospheric versus
892 vegetation controls of Amazonian tropical rain forest evapotranspiration: Are the wet and
893 seasonally dry rain forests any different?, J. Geophys. Res. – Biogeosci., 115, G04021,
894 doi: 10.1029/2009JG001179, 2010.
895 Cox, P.M., Betts, R.A., Jones, C.D., Spall, S.A., and Totterdell, I.J.: Acceleration of global
896 warming due to carbon-cycle feedbacks in a coupled climate model, Nature, 408, 184 –
897 187, 2000.
898 da Rocha, H.R., Manzi, A.O., Cabral, O.M. et al.: Patterns of water and heat flux across a
899 biome gradient from tropical forest to savanna in Brazil. J. Geophys. Res. – Biogeosci.,
900 114, G00B12, doi:10.1029/2007JG000640, 2009.
901 da Rocha, H.R., Goulden, M., Miller, S., Menton, M., Pinto, L., Freitas, H., and Figueira,
902 A.S.: Seasonality of water and heat fluxes over a tropical forest in eastern Amazonia,
903 Ecol. Appl., 14(4), 22– 32, 2004.

Davidson, E.A., de Araújo, A.C., Artaxo, P. et al.: The Amazon basin in transition, *Nature*, 481(7381), 321–328, 2012.

Denmead, O.T., and Shaw, R.H.: Availability of soil water to plants as affected by soil moisture content and meteorological conditions, Agron. J., 54, 385–390, 1962.

Dolman, A.J., Miralles, D.G., and de Jeu, R.A.M.: Fifty years since Monteith's 1965 seminal paper: the emergence of global ecohydrology, Ecohydrol., 7, 897–902, doi: 10.1002/eco.1505, 2014.

Drewry, D.T., Kumar, P., Long, S., Bernacchi, C., Liang, X.Z., and Sivapalan, M.: Ecohydrological responses of dense canopies to environmental variability: 1. Interplay between vertical structure and photosynthetic pathway, J. Geophys. Res. – Biogeosci., 115, G04022, doi:10.1029/2010JG001340, 2010.

Ershadi, A., et al.: Impact of model structure and parameterization on Penman–Monteith type evaporation models, J Hydrol. 525, 521 – 535, 2015.

Foken, T.: 50 Years of the Monin-Obukhov similarity theory, Boundary-Layer Meteorol., 2, 7–29, 2006.

Gatti, L.V., Gloor, M., Miller, J.B., et al.: Drought sensitivity of Amazonian carbon balance revealed by atmospheric measurements, Nature, 506, 76–80, doi: 10.1038/nature12957, 2014.

Gibson, L. A., Münch, Z., and Engelbrecht, J.: Particular uncertainties encountered in using a pre-packaged SEBS model to derive evapotranspiration in a heterogeneous study area in South Africa, Hydrol. Earth Syst. Sci., 15, 295-310, doi:10.5194/hess-15-295-2011, 2011.

Gloor, M., Brienen, R.J.W., Galbraith, D., et al.: Intensification of the Amazon hydrological cycle over the last two decades, Geophys. Res. Let., 40, 1729–1733, 2013.

de Goncalves, L.G.G., Borak, J.S., Costa, M.H., Saleska, S.R., et al.: Overview of the Large-Scale Biosphere–Atmosphere Experiment in Amazonia Data Model Intercomparison Project (LBA-DMIP), Agric. For. Meteorol., 182– 183, 111– 127, 2013.

Harper, A., Baker, I.T., Denning, A.S., Randall, D.A., Dazlich, D., and Branson, M.: Impact of Evapotranspiration on Dry Season Climate in the Amazon Forest, J. Climate, 27, 574–591, doi: http://dx.doi.org/10.1175/JCLI-D-13-00074.1, 2014.

Hasler, N., and Avissar, R.: What controls evapotranspiration in the Amazon Basin, J. Hydrometeorol., 8, 380–395, doi: http://dx.doi.org/10.1175/JHM587.1, 2007.

Hilker, T., Lyapustin, A.I., Tucker, C.J., et al.: Vegetation dynamics and rainfall sensitivity of the Amazon, Proc. National Academy of Sci., 111 (45), 16041 – 16046, doi: 10.1073/pnas.1404870111, 2014.

Holwerda, F., Bruijnzeela, L.A., Scatenac, F.N., Vugtsa, H.F., and Meestersa, A.G.C.A.: Wet canopy evaporation from a Puerto Rican lower montane rain forest: the importance of realistically estimated aerodynamic conductance, J. Hydrol., 414-415, 1-15, 2012.

Huband, N.D.S., and Monteith, J.L.: Radiative surface temperature and energy balance of a wheat canopy I: Comparison of radiative and aerodynamic canopy temperature, Boundary-Layer Meteorol., *36*, 1-17, 1986.

Huntingford, C., Fisher, R.A., Mercado, L., et al.: Towards quantifying uncertainty in predictions of Amazon 'dieback', Phil. Trans. Royal Soc. London. Ser. B, Biol. Sci., 363, 1857–1864, 2008.

Jarvis, P. G.: The interpretation of leaf water potential and stomatal conductance found in canopies in the field, Philos. Trans. R. Soc. London B, 273, 593–610, 1976.

Jarvis, P.G.: Transpiration and assimilation of trees and agricultural crops: the 'omega' factor. In *Attributes of Trees and Crop Plants,* Edited by Cannell MGR and Jackson JE, Institute of terrestrial Ecology, Edinburg, UK, 460 – 480, 1986.

Jarvis, P.G., and McNaughton, K.G.: Stomatal control of transpiration: scaling up from leaf to region, Adv. Ecol. Res., 15, 1 – 49, 1986.

Jones, H.G.: Stomatal control of photosynthesis and transpiration, J. Exp. Bot., 49, 387 – 398, 1998.

Kumagai, T., et al.: Transpiration, canopy conductance and the decoupling coefficient of a lowland mixed dipterocarp forest in Sarawak, Borneo: dry spell effects, J. Hydrol., 287, 237–251, 2004.

Kustas, W.P., and Anderson, M.C.: Advances in thermal infrared remote sensing for land surface modeling, Agric. For. Meteorol., 149, 2071 – 2081, 2009.

Lawrence, D., and Vandecar, K.: Effects of tropical deforestation on climate and agriculture, Nature Clim. Change, 5, 27–36, doi: 10.1038/nclimate2430, 2015.

Leuning, R.: A critical appraisal of a combined stomatal – photosynthesis model for c3 plants, Pl. Cell and Environ., 18, 339 – 355, 1995.

Leuzinger, S., and Kirner, C.: Rainfall distribution is the main driver of runoff under future CO2-concentration in a temperate deciduous forest, Global Change Biol., 16, 246 – 254, 2010.

Lhomme, J.P., and Montes, C.: Generalized combination equations for canopy evaporation under dry and wet conditions, Hydrol. Earth Sys. Sci., 18, 1137–1149, 2014.

Loescher, H.W., Gholz, H.L., Jacobs, J.M., and Oberbauer, S.F.: Energy dynamics and modeled evapotranspiration from a wet tropical forest in Costa Rica, J. Hydrol., 315, 274 – 294, 2005.

974 Ma, N., et al.: Environmental and biophysical controls on the evapotranspiration over the
975 highest alpine steppe, J. Hydrol., 529 (3), 980–992, 2015.
976 Malhi, Y., Pegoraro, E., Nobre, A.D., Pereira, M.G.P., Grace, J., Culf, A.D., and Clement, R.:
977 The energy and water dynamics of a central Amazonian rain forest, J. Geophys. Res.,
978 107, D20, 10.1029/2001JD000623, 2002.
979 Malhi, Y.: The productivity, metabolism and carbon cycle of tropical forest vegetation, J.
980 Ecol., 100, 65–75, 2012.
981 Mallick, K., Boegh, E., Trebs, I., et al.: Reintroducing radiometric surface temperature into
982 the Penman-Monteith formulation, Water Resour. Res., 51,
983 doi:10.1002/2014WR016106, 2015.
984 Mallick, K., Jarvis, A.J., Boegh, E., et al.: A surface temperature initiated closure (STIC) for
985 surface energy balance fluxes, Remote Sens. Environ., 141, 243 – 261, 2014.
986 Massman, W. J.: A model study of kB_H^{-1} for vegetated surfaces using 'localized near-field'
987 Lagrangian theory, J. Hydrol., 223, 27-43, 1999.
988 Matheny, A.M., Bohrer, G., Stoy, P., Baker, I.T., et al.: Characterizing the diurnal patterns of
989 errors in the prediction of evapotranspiration by several land-surface models: An NACP
990 analysis, J. Geophys. Res.- Biogeosci., 119, doi:10.1002/2014JG002623, 2014.
991 Matzner, S., and Comstock, J.: The temperature dependence of shoot hydraulic resistance:
992 implications for stomatal behaviour and hydraulic limitation, Pl. Cell and Environ., 24
993 (11), 1299 – 1307, 2001.
994 McNaughton, K.G., and Jarvis, P.G.: Using the Penman-Monteith equation predictively,
995 Agric. Water Management, 8 (1-3), 263-278, 1984.
996 McNaughton, K.G., and Jarvis, P.G.: Effects of spatial scale on stomatal control of
997 transpiration, Agric. For. Meteorol., 54, 279 – 301, 1991.

998 Medlyn, B.E., Duursma, R.A., Eamus, D., et al.: Reconciling the optimal and empirical
999 approaches to modelling stomatal conductance, Global Change Biol., doi:
1000 10.1111/j.1365-2486.2010.02375.x, 2011.

1001 Meinzer, F.C., Andrade, J.L., Goldstein, G., Holbrook, N.M., Cavelier, J., and Jackson, P.:
1002 Control of transpiration from upper canopy of a tropical forest: the role of stomatal,
1003 boundary layer and hydraulic architecture components, Pl. Cell and Environ., 20, 1242 –
1004 1252, 1997.

1005 Meinzer, F.C., Goldstein, G., Holbrook, N.M., Jackson, P., Cavelier, J.: Stomatal and
1006 environmental control of transpiration in a lowland tropical forest site, Pl. Cell and
1007 Environ., 16, 429 – 436, 1993.

1008 Mercado, L.M., Lloyd, J., Dolman, A.J., Sitch, S., and Pati, S.: Modelling basin-wide
1009 variations in Amazon forest productivity – Part 1: Model calibration, evaluation and
1010 upscaling functions for canopy photosynthesis, Biogeosci., 6, 1247-1272, doi:
1011 10.5194/bg-6-1247-2009, 2009.

1012 Miglietta, F., Peressotti, A., Viola, R., Körner, C., and Amthor, J.S.: Stomatal numbers, leaf
1013 and canopy conductance, and the control of transpiration, Proc. National Acad. Sci., 108
1014 (28), E275-E275, 2011.

1015 Monteith, J.L.: Evaporation and environment. In G.E. Fogg (ed.) *Symposium of the Society*
1016 *for Experimental Biology, The State and Movement of Water in Living Organisms*, *19*,
1017 pp. 205-234. Academic Press, Inc., NY, 1965.

1018 Monteith, J.L.: Evaporation and surface temperature, Quart. J. Royal Met. Soc., 107, 1–27,
1019 1981.

1020 Monteith, J.L.: Accommodation between transpiring vegetation and the convective boundary
1021 layer, J. Hydrol., 166, 251 – 263, 1995.

1022 Monteith, J.L., and Unsworth, M.H.: *Principles of Environmental Physics*. Elsevier,
1023 Amsterdam, 2008.
1024 Moran, M.S., Clarke, T.R., Inoue, Y., Vidal, A.: Estimating crop water deficit between
1025 surface-air temperature and spectral vegetation index, Remote Sens. Environ., 46, 246-
1026 263, 1994.
1027 Motzer, T., Munz, N., Kuppers, M., Schmitt, D., and Anhuf, D.: Stomatal conductance,
1028 transpiration and sap flow of tropical montane rain forest trees in the southern
1029 Ecuadorian Andes, Tree Physiol., 25, 1283 – 1293, 2005.
1030 O'Grady, A.P., Eamus, D., and Hutley, L. B.: Transpiration increases during the dry season:
1031 patterns of tree water use in eucalypt open-forests of northern Australia, Tree Physiol.,
1032 19, 591—597, 1999.
1033 Penman, H.L.: Natural evaporation from open water, bare soil, and grass, Proc. Royal Soc.
1034 London, Ser. A, 193, 120–146, 1948.
1035 Priante Filho, N., Vourlitis, G.L., Hayashi, M.M.S., de Souza Nogueira, J., et al.: Comparison
1036 of the mass and energy exchange of a pasture and a mature transitional tropical forest of
1037 the southern Amazon Basin during a seasonal transition, Global Change Biol., 10, 863–
1038 876, doi: 10.1111/j.1529-8817.2003.00775.x, 2004.
1039 Priestley, C.H.B., and Taylor, R.J.: On the assessment of surface heat flux and evaporation
1040 using large scale parameters, Monthly Weather Rev., 100, 81–92, 1972.
1041 Prihodko, L., Denning, A.S., Hanan, N.P., Baker, I.T., and Davis, K.: Sensitivity, uncertainty
1042 and time dependence of parameters in a complex land surface model, Agric. For.
1043 Meteorol., 148 (2), 268–287, 2008.
1044 Raupach, M.R.: Vegetation-atmosphere interaction and surface conductance at leaf, canopy
1045 and regional scales, Agric. For. Meteorol., 73, 151-179, 1995.

1046 Raupach, M.R., and Finnigan, J.J.: Scale issues in boundary-layer meteorology: surface
1047 energy balance in heterogeneous terrain, Hydrol. Proc., 9, 589 – 612, 1995.
1048 Raupach, M.R..: Influence of local feedbacks on land-air exchanges of energy and carbon,
1049 Global Change Biol., 4, 477 – 494, 1998.
1050 Renner, M., Hassler, S.K., Blume, T., Weiler, M., et al.: Dominant controls of transpiration
1051 along a hillslope transect inferred from ecohydrological measurements and
1052 thermodynamic limits, Hydrol. Earth Syst. Sci., 20, 2063-2083, doi:10.5194/hess-20-
1053 2063-2016, 2016.
1054 Richiardone, R., Manfrin, M., Ferrarese, S., Francone, C., Fernicola, V., Gavioso, R.M., and
1055 Mortarini, L.: Influence of the Sonic Anemometer Temperature Calibration on Turbulent
1056 Heat-Flux Measurements, Boundary Layer Meteorol., 142 (3), 425-442, 2012.
1057 Roy, S.B., and Avissar, R.: Impact of land use/land cover change on regional
1058 hydrometeorology in Amazonia, J. Geophys. Res., 107, D20, doi:
1059 10.1029/2000JD000266, 2002.
1060 Restrepo-Coupea, N., da Rocha, H.R., Hutyra, L.R., da Araujo, A.C., et al.: What drives the
1061 seasonality of photosynthesis across the Amazon basin? A cross-site analysis of eddy
1062 flux tower measurements from the Brasil flux network, Agric. For. Meteorol., 182– 183,
1063 128– 144, 2013.
1064 Ocheltree, T.W., Nippert, J.B., and Prasad, P.V.V.: Stomatal responses to changes in vapor
1065 pressure deficit reflect tissue-specific differences in hydraulic conductance, Pl. Cell
1066 Environ., 37, 132–139, 2014.
1067 Saleska, S.R., da Rocha, H.R., Huete, A.R., Nobre, A.D., Artaxo, P., and Shimabukuro, Y.E.:
1068 LBA-ECO CD-32 Flux Tower Network Data Compilation, Brazilian Amazon: 1999-
1069 2006. Data set. Available on-line [http://daac.ornl.gov] from Oak Ridge National

Laboratory Distributed Active Archive Center, Oak Ridge, Tennessee, USA, http://dx.doi.org/10.3334/ORNLDAAC/1174, 2013.

Shuttleworth, W. J., Gurney, R. J., Hsu, A. Y., and Ormsby, J. P.: FIFE: The variation in energy partition at surface flux sites, in Remote Sensing and Large Scale Processes, Proceedings of the IAHS Third International Assembly, vol. 186, edited by A. Rango, pp. 67–74, IAHS Publ., Baltimore, Md, 1989.

Shuttleworth, W.J.: Micrometeorology of temperate and tropical forest, Phil. Trans. Royal Soc. London. Ser. B, Biol. Sci., 324, 299-334, 1989.

Shuttleworth, W.J.: Putting the "vap" into evaporation. Hydrol. Earth Sys. Sci., 11, 210-244, doi: 10.5194/hess-11-210-2007, 2007.

Shuttleworth, W.J., and Wallace, J.S.: Evaporation from sparse crops – an energy combination theory, Quart. J. Royal Met. Soc., 111, 839 – 855, 1985.

Simpson, I.J., Thurtell, G.W., Nuemann, H.H., den Hartog, G., Edwards, G.C.: The validity of similarity theory in the roughness sublayer above forests, Boundary- Layer Meteorology 87, 69-99, 1998.

Stella, P., Kortner, M., Ammann, C., Foken, T., Meixner, F. X., and Trebs, I.: Measurements of nitrogen oxides and ozone fluxes by eddy covariance at a meadow: evidence for an internal leaf resistance to NO2, Biogeosci., 10, 5997-6017, doi:10.5194/bg-10-5997-2013, 2013.

Streck, N.A.: Stomatal response to water vapor pressure deficit: an unsolved issue, Revista Brasil. Agrociên., 9 (4), 317–322, 2003.

Thom, A.S., Stewart, J.B., Oliver, H.R., Gash, J.H.C.: Comparison of aerodynamic and energy budget estimates of fluxes over a pine forest, Quart. J. Royal Met. Soc., 101, 93-105, 1975.

1094 Tuzet, A., Perrier, A., and Leuning, R.: A coupled model of stomatal conductance,
1095 photosynthesis and transpiration, Pl. Cell Environ., 26, 1097–1116, 2003.
1096 van der Tol, C., van der Tol, S., Verhoef, A., Su, B., Timmermans, J., Houldcroft, C., and
1097 Gieske, A.: A Bayesian approach to estimate sensible and latent heat over vegetated land
1098 surface, Hydrol. Earth Sys. Sci., 13, 749–758, doi:10.5194/hess-13-749-2009, 2009.
1099 Van Dijk, A.I.J.M., et al.: Rainfall interception and the couple surface water and energy
1100 balance, Agric. For. Meteorol., 214 – 215, 402 – 415, 2015.
1101 Venturini, V., Islam, S., and Rodriguez, L.: Estimation of evaporative fraction and
1102 evapotranspiration from MODIS products using a complementary based model, Remote
1103 Sens. Environ., 112(1), 132-141, 2008.
1104 von Randow, R.C.S., von Randow, C., Hutjes, R.W.A., Tomasella, J., and Kruijt, B.:
1105 Evapotranspiration of deforested areas in central and southwestern Amazonia, Theor.
1106 Appl. Climatol., 109:205–220, doi: 10.1007/s00704-011-0570-1, 2012.
1107 Villagarcía, L., Were, A., García, M., and Domingo, F.: Sensitivity of a clumped model of
1108 evapotranspiration to surface resistance parameterisations: Application in a semi-arid
1109 environment, Agric. For. Meteorol., 150 (7), 1065-1078, 2010.
1110 Villani, M.G., Schmid, H.P., Su, H.B., Hutton, J.L., and Vogel, C.S.: Turbulence statistics
1111 measurements in a northern hardwood forest, Boundary-Layer Meteorology 108: 343–
1112 364, 2003.
1113 Zhang, Q., Manzoni, S., Katul, G., Porporato, A., and Yang, D.: The hysteretic
1114 evapotranspiration-vapor pressure deficit relation, J. Geophys. Res. Biogeosci., 119,
1115 125–140, doi:10.1002/2013JG002484, 2014.
1116
1117

1118 **Table 1:** Variables and symbols and their description used in the study

Variables and symbol	Description
λE	Evapotranspiration (evaporation + transpiration) as latent heat flux (W m^{-2})
H	Sensible heat flux (W m^{-2})
R_N	Net radiation (W m^{-2})
G	Ground heat flux (W m^{-2})
ϕ	Net available energy (W m^{-2})
T_A	Air temperature (ºC)
T_D	Dewpoint temperature (ºC)
T_R	Radiometric surface temperature (ºC)
R_H	Relative humidity (%)
e_A	Atmospheric vapor pressure at the level of T_A measurement (hPa)
D_A	Atmospheric vapor pressure deficit at the level of T_A measurement (hPa)
W_S	Wind speed (m s^{-1})
u^*	Friction velocity (m s^{-1})
T_{SD}	Dew-point temperature at the source/sink height (ºC)
T_0	Aerodynamic surface temperature or source/sink height temperature (ºC)
e_S	'effective' vapor pressure of evaporating front near the surface (hPa)
e_S^*	Saturation vapor pressure of surface (hPa)
e_0^*	Saturation vapor pressure at the source/sink height (hPa)
e_0	Atmospheric vapor pressure at the source/sink height (hPa)
D_0	Atmospheric vapor pressure deficit at the source/sink height (hPa)
λE_{eq}	Equilibrium latent heat flux (W m^{-2})
λE_{imp}	Imposed latent heat flux (W m^{-2})
λE_E	Evaporation as flux (W m^{-2})
λE_T	Transpiration flux (W m^{-2})
E	Evapotranspiration (evaporation + transpiration) as depth of water (mm)
λE^*	Potential evaporation as flux (W m^{-2})
λE_T^*	Potential transpiration as flux (W m^{-2})
λE_W	Wet environment evaporation as flux (W m^{-2})
λE_P^*	Potential evaporation as flux according to Penman (W m^{-2})
λE_{PM}^*	Potential evaporation as flux according to Penman-Monteith (W m^{-2})
λE_{PT}^*	Potential evaporation as flux according to Priestley-Taylor (W m^{-2})
E^*	Potential evaporation as depth of water (mm)
E_P^*	Potential evaporation as depth of water according to Penman (mm)
E_{PM}^*	Potential evaporation as depth of water according to Penman-Monteith (mm)
E_{PT}^*	Potential evaporation as depth of water according to Priestley-Taylor (mm)
E_W	Wet environment evaporation as depth of water (mm)
g_A	Aerodynamic conductance (m s^{-1})
g_C	Stomatal / surface conductance (m s^{-1})
g_M	Momentum conductance (m s^{-1})
g_B	Quasi-laminar boundary layer conductance (m s^{-1})
g_{Smax}	Maximum stomatal / surface conductance (m s^{-1}) (= g_S/M)

M	Surface moisture availability (0 – 1)
s	Slope of saturation vapor pressure versus temperature curve (hPa K^{-1}) (estimated at T_A)
s_1	Slope of the saturation vapor pressure and temperature between ($T_{SD} - T_D$) versus ($e_0 - e_A$) (approximated at T_D) (hPa K^{-1})
s_2	Slope of the saturation vapor pressure and temperature between ($T_R - T_D$) versus ($e_S^* - e_A$) (hPa K^{-1})
s_3	Slope of the saturation vapor pressure and temperature between ($T_R - T_{SD}$) versus ($e_S^* - e_S$) (approximated at T_R) (hPa K^{-1})
κ	Ratio between ($e_0^* - e_A$) and ($e_S^* - e_A$)
λ	Latent heat of vaporization of water (j $kg^{-1}K^{-1}$)
z_R	Reference height (m)
z_M	Effective source-sink height of momentum (m)
z_0	Roughness length (m)
d	Displacement height (m)
γ	Psychrometric constant (hPa K^{-1})
ρ	Density of air (kg m^{-3})
c_p	Specific heat of dry air (MJ kg^{-1} K^{-1})
Λ	Evaporative fraction (unitless)
β	Bowen ratio (unitless)
α	Priestley-Taylor parameter (unitless)
Ω	Decoupling coefficient (unitless)
S_c	Schmidt number (unitless)
P_r	Prandtl number (unitless)
k	Von Karman's constant (0.4)

Table 2: Overview of the LBA tower sites.

Biome	PFT	Site	LBA Code	Data availability period	Latitude	Longitude	Tower height (m)	Annual rainfall (mm)
Forest	Tropical rainforest (TRF)	Manaus KM34	K34	06/1999 to 09/2006	-2.609	-60.209	50	2329
Forest	Tropical moist forest (TMF)	Santarem KM67	K67	01/2002 to 01/2006	-2.857	-54.959	63	1597
Forest	Tropical moist forest (TMF)	Santarem KM83	K83	07/2000 to 12/2004	-3.018	-54.971	64	1656
Forest	Tropical dry forest (TDF)	Reserva Biológica Jarú	RJA	03/1999 to 10/2002	-10.083	-61.931	60	2354
Pasture	Pasture (PAS)	Santarem KM77	K77	01/2000 to 12/2001	-3.012	-54.536	18	1597
Pasture	Pasture (PAS)	Fazenda Nossa Senhora	FNS	03/1999 to 10/2002	-10.762	-62.357	8.5	1743

Table 3: Comparative statistics for the STIC and tower-derived hourly g_A and g_C for a range of PFTs in the Amazon Basin (LBA tower sites). Values in parenthesis are ± one standard deviation (standard error for correlation).

PFTs	$g_{A\text{-}STIC}$ vs. $g_{A\text{-}BM13}$					$g_{C\text{-}STIC}$ vs. $g_{C\text{-}INV}$			
	RMSD ($m\ s^{-1}$)	R^2	Slope	Offset ($m\ s^{-1}$)	N	RMSD ($m\ s^{-1}$)	R^2	Slope	Offset ($m\ s^{-1}$)
TRF	0.013	0.41 (±0.03)	1.07 (±0.047)	0.0031 (±0.0008)	1159	0.012	0.14 (±0.04)	0.39 (±0.039)	0.0097 (±0.0007)
TMF	0.012	0.55 (±0.12)	0.81 (±0.023)	0.0006 (±0.0006)	1927	0.009	0.55 (±0.12)	0.85 (±0.025)	0.0032 (±0.0005)
TDF	0.007	0.49 (±0.15)	0.89 (±0.041)	0.0019 (±0.0006)	787	0.012	0.33 (±0.19)	0.30 (±0.022)	0.0050 (±0.0005)
PAS	0.012	0.22 (±0.18)	1.03 (±0.083)	0.0059 (±0.0007)	288	0.007	0.58 (±0.12)	0.65 (±0.025)	0.0024 (±0.0003)
Mean	**0.012**	**0.44 (**±0.10**)**	**0.76 (**±0.016**)**	**0.0047** (±0.003)	**4161**	**0.010**	**0.39 (**±0.08**)**	**0.63 (**±0.016**)**	**0.0046 (**±0.0003**)**

N = number of data points; RMSD = root mean square deviation between predicted (P) and observed (O) variables = $\left[\frac{1}{N}\sum_{i=0}^{N}(P_i - O_i)^2\right]^2$.

Table 4: Comparative statistics for the STIC and tower-derived hourly λE and H for a range of PFTs in the Amazon Basin (LBA tower sites). Values in parenthesis are ±one standard deviation (standard error for correlation).

PFTs	λE				H				
	RMSD ($W\ m^{-2}$)	R^2	Slope	Offset ($W\ m^{-2}$)	RMSD ($W\ m^{-2}$)	R^2	Slope	Offset ($W\ m^{-2}$)	N
TRF	28	0.96 (±0.007)	1.10 (±0.008)	-16 (±2)	34	0.52 (±0.030)	0.60 (±0.025)	29 (±2)	1159
TMF	20	0.98 (±0.004)	1.08 (±0.004)	-11 (±1)	23	0.71 (±0.019)	0.61 (±0.014)	20 (±1)	1927
TDF	26	0.96 (±0.009)	0.96 (±0.008)	-7 (±2)	30	0.66 (±0.032)	0.89 (±0.035)	20 (±3)	787
PAS	31	0.96 (±0.009)	1.14 (±0.010)	-2 (±2)	33	0.88 (±0.016)	0.67 (±0.011)	9 (±1)	288
Mean	**33**	**0.94 (±0.005)**	**1.04 (±0.005)**	**-1 (±1)**	**37**	**0.61 (±0.021)**	**0.58 (±0.009)**	**24 (±2)**	**4161**

Figure 1. Examples of monthly averages of the diurnal time series of canopy-scale (a) g_A and (b) g_C estimated for two different biomes (forest and pasture) in the Amazon Basin (LBA sites K34 and FNS). The time series of four different g_A estimates and their corresponding g_C estimates are shown here.

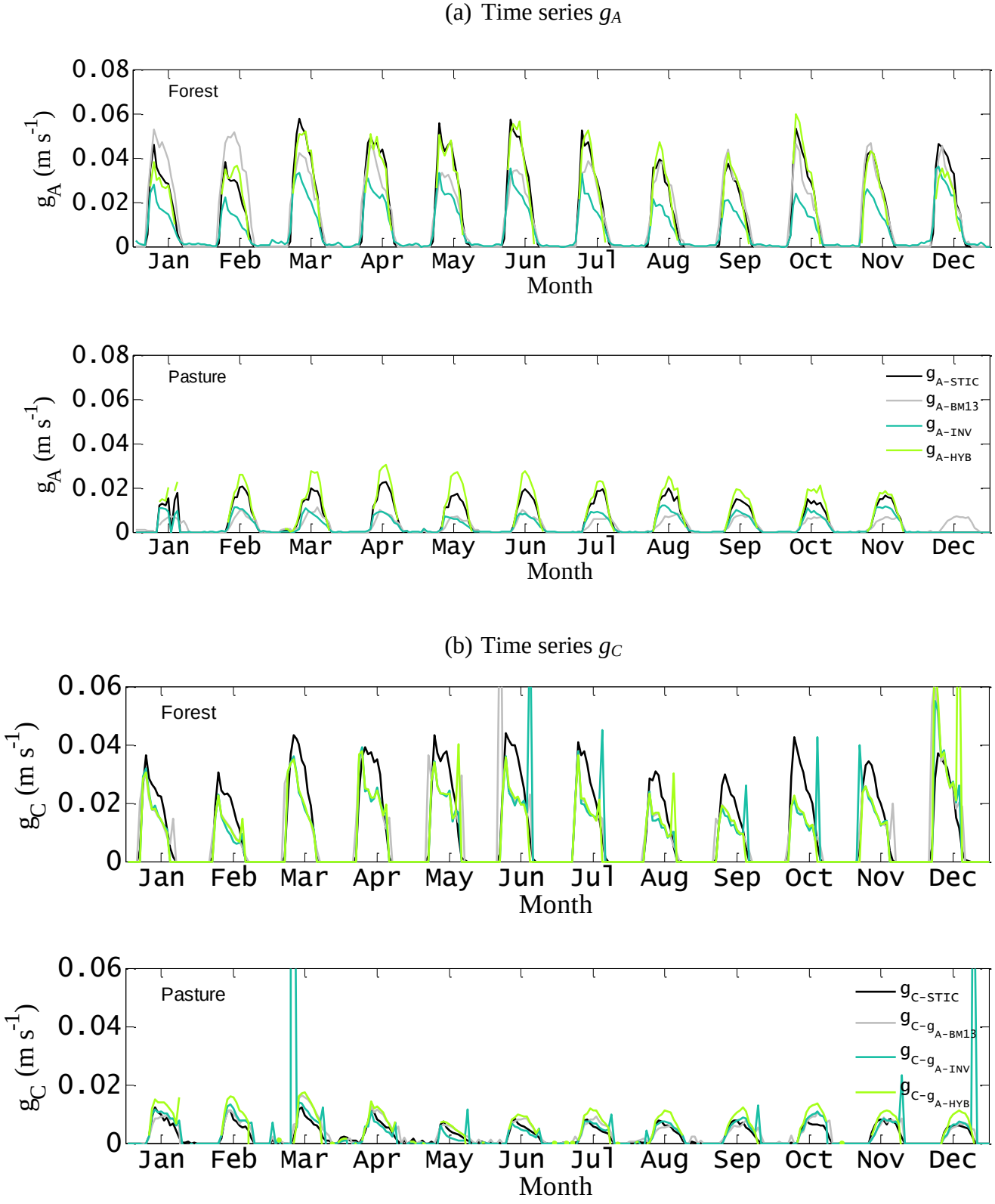

Figure 2. (a) Comparison between STIC derived g_A ($g_{A\text{-}STIC}$) with an estimated aerodynamic conductance based on friction velocity (u^*) and wind speed (u) according to Baldocchi and Ma (2013) ($g_{A\text{-}BM13}$), (b) Comparison between $g_{A\text{-}STIC}$ with an inverted g_A ($g_{A\text{-}INV}$) based on EC observations of λE and D_A, (c) Comparison between $g_{A\text{-}STIC}$ with a hybrid g_A ($g_{A\text{-}HYB}$) based on EC observations of H and estimated T_0 over the LBA EC sites, (d) Comparison between residual g_A differences versus u and u^*, (e) and (f) Relationship between wind and shear derived g_A versus ϕ, T_R, and D_A over the LBA EC sites.

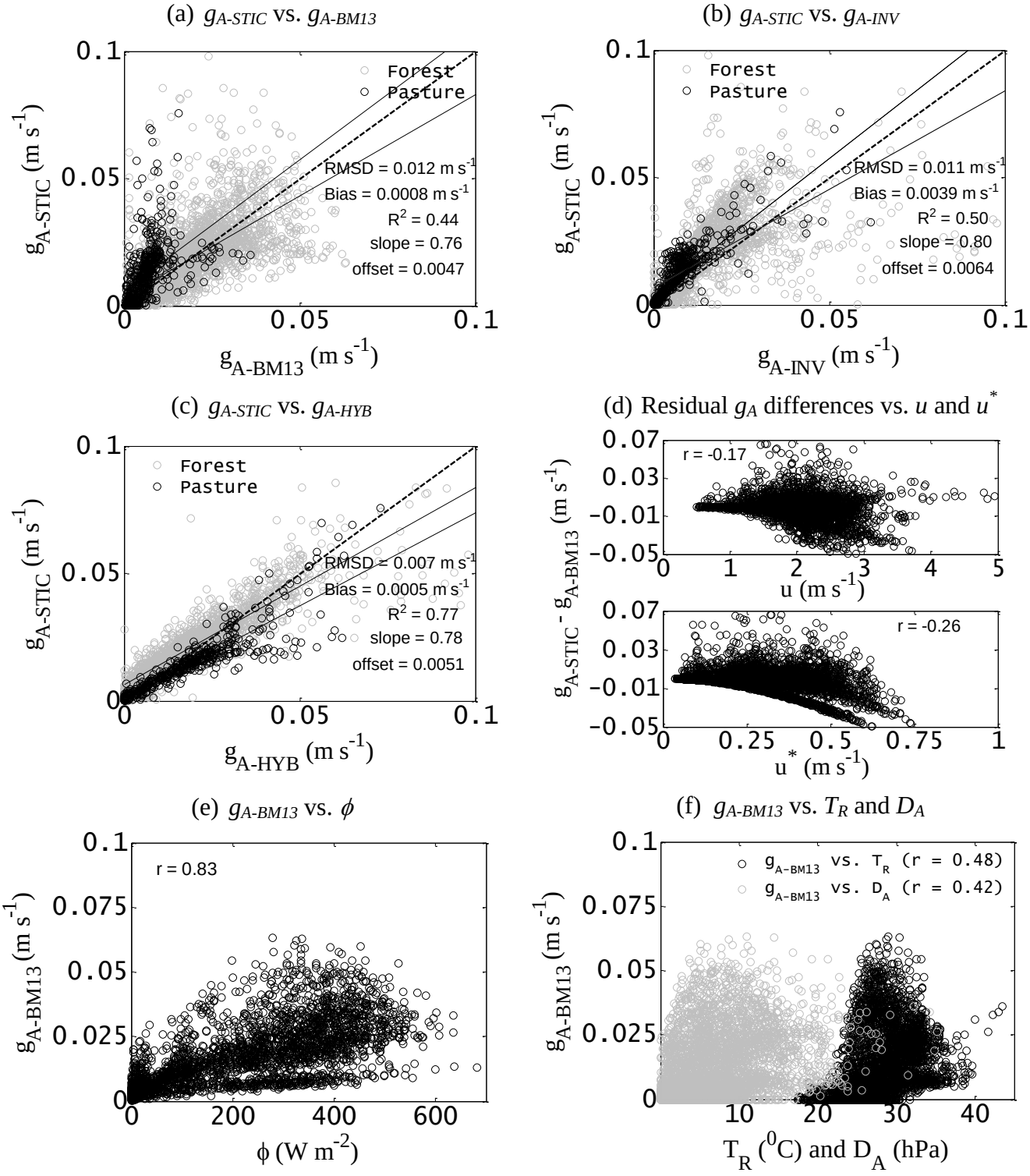

Figure 3. (a) Comparison between STIC derived g_C ($g_{C\text{-}STIC}$) and g_C computed by inverting the PM model ($g_{C\text{-}INV}$) over the LBA EC sites, where $g_{A\text{-}BM13}$ was used as aerodynamic input in conjunction with tower measurements of λE, radiation and meteorological variables, (b) Residual g_C differences versus wind speed (u) and friction velocity (u^*) over the LBA EC sites.

(a) Tower scale evaluation of g_C

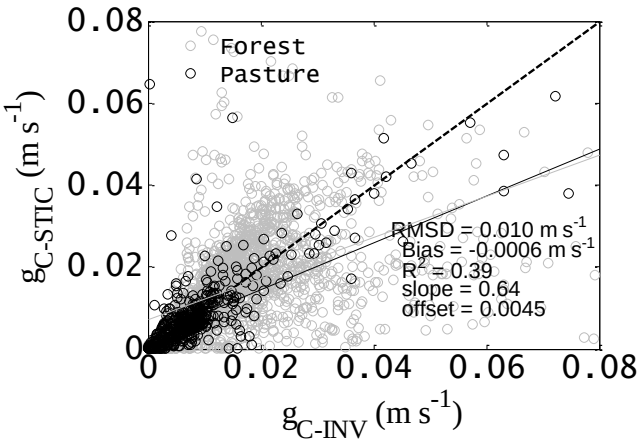

(b) Residual g_C differences vs. u and u^*

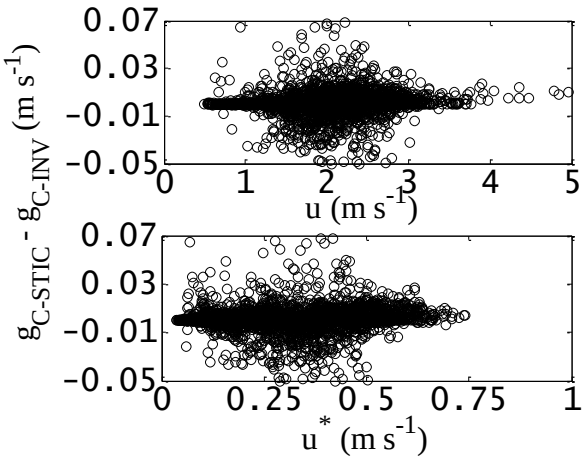

Figure 4. Comparison between STIC derived (a) λE and (b) H over four different PFTs in the Amazon Basin (LBA tower sites). MAPD is the percent error defined as the mean absolute deviation between predicted and observed variable divided by mean observed variable.

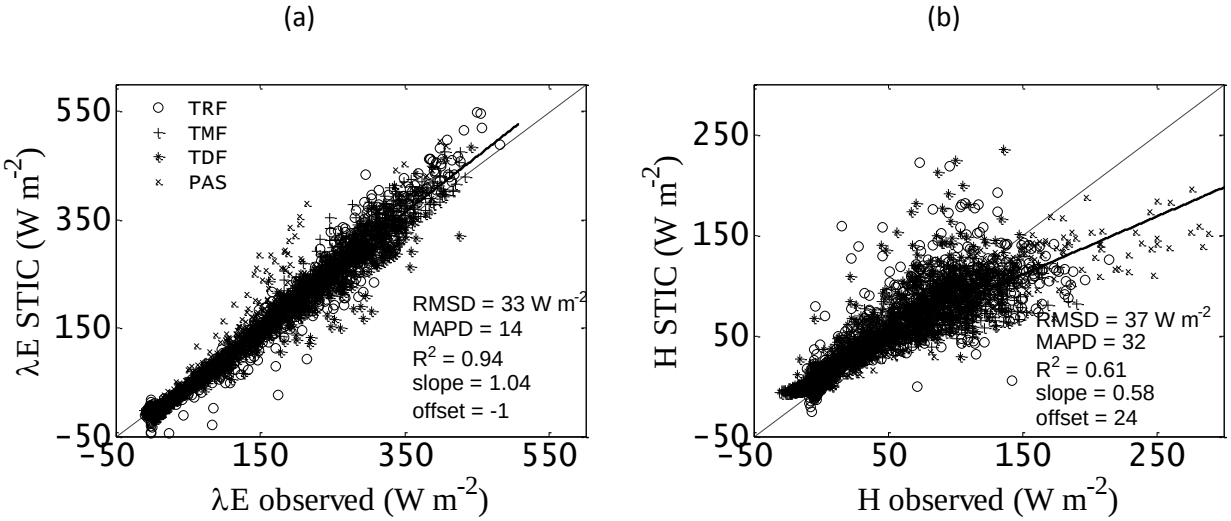

Figure 5. Correlation of coupling (1-Ω) with (a) transpiration (λE_T) and (b) evaporation (λE_E) and over four different PFTs by combining data for all the years, only during dry seasons for all the years, and during drought year 2005. Data for 2005 was not available for TDF and PAS. (c) to (e) Examples of diurnal pattern of Ω (black lines), λE_E (grey dotted lines) and λE_T (grey solid lines) estimated over two ecohydrologically contrasting biomes (K34 for forest and FNS for pasture) in the Amazon Basin (LBA tower sites) during wet and dry seasons.

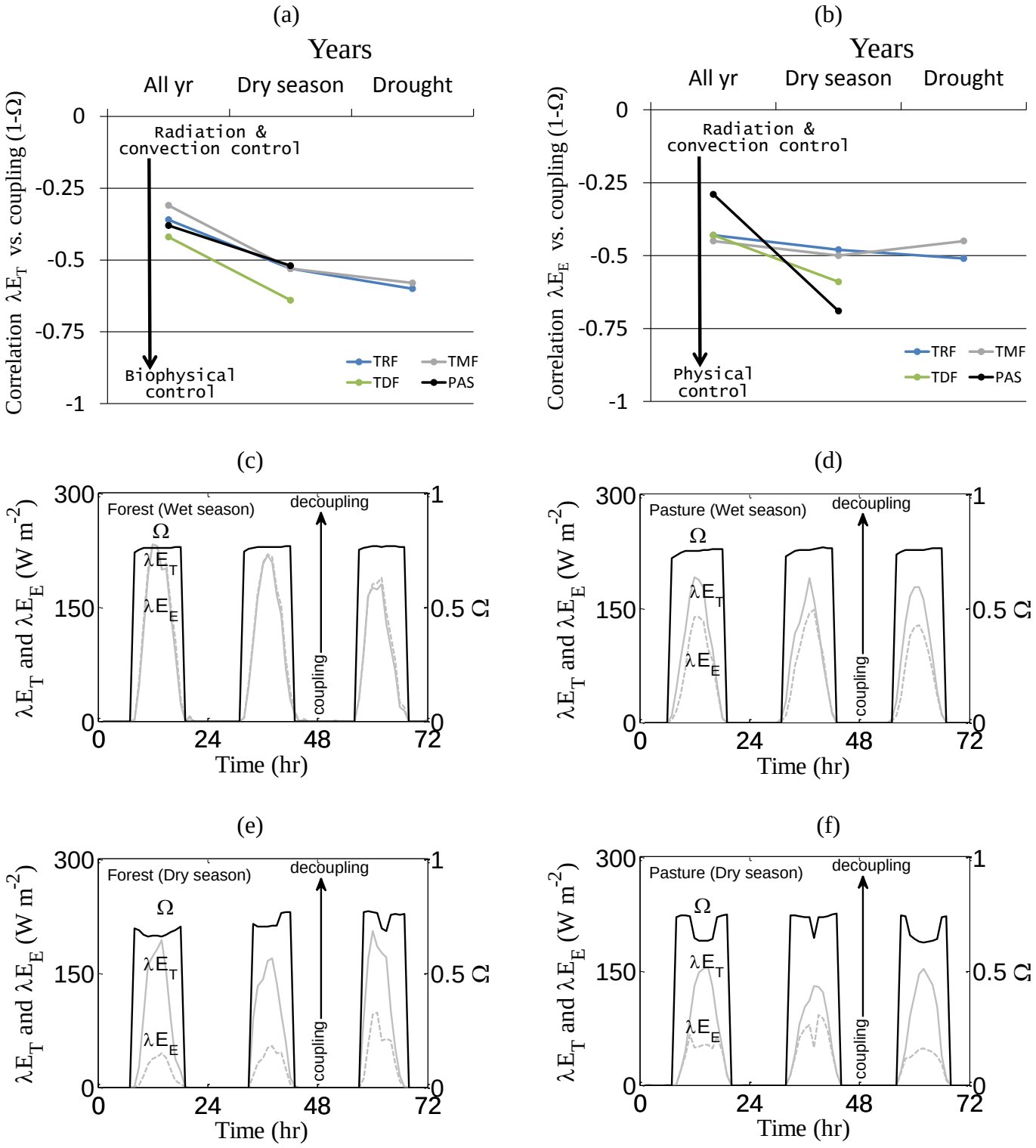

Figure 6. Scatter plots of transpiration (λE_T) and evaporation (λE_E) versus g_C and g_A over four different PFTs in the Amazon Basin (LBA tower sites).

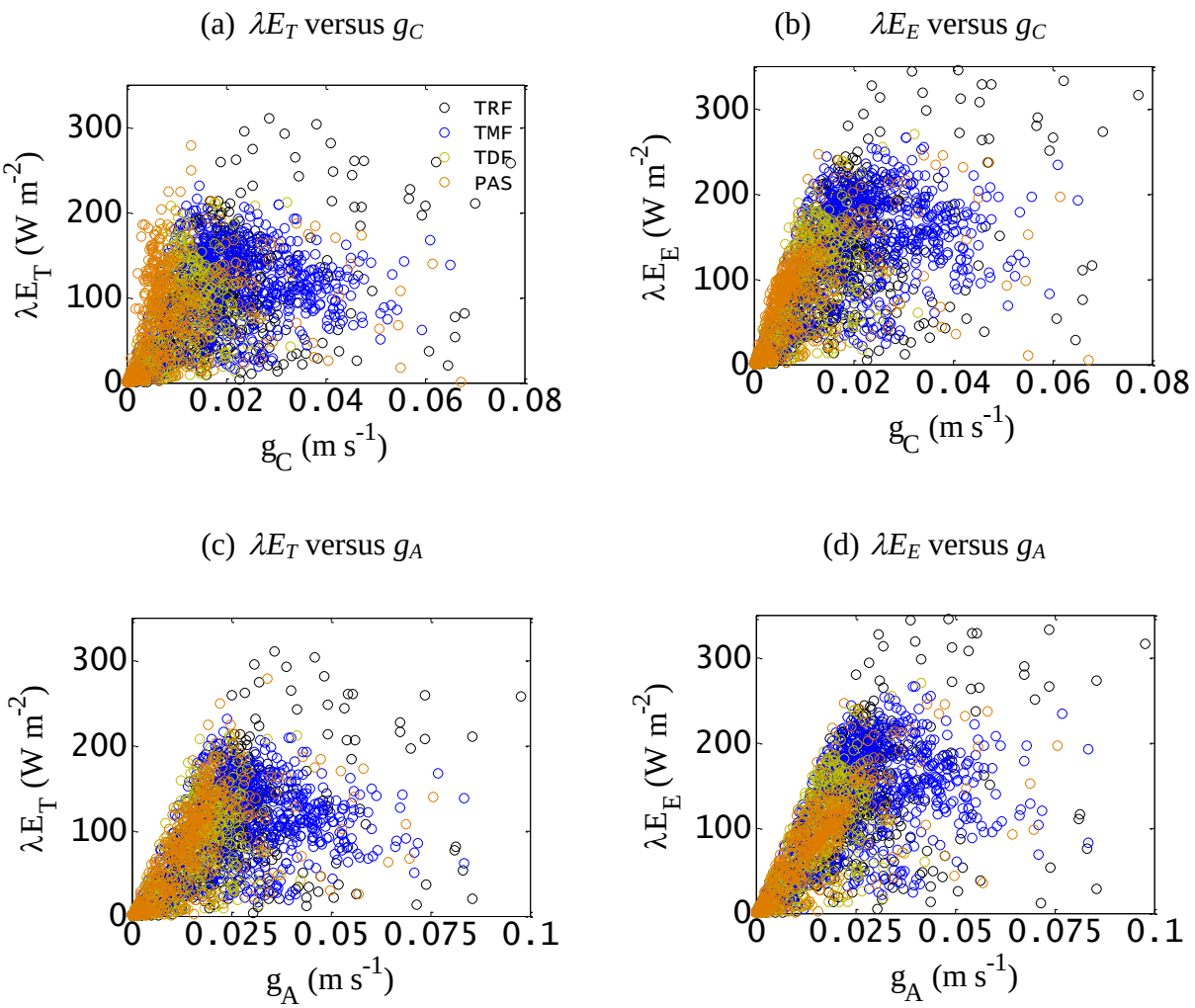

Figure 7. Illustrative examples of the occurrence of diurnal hysteresis of transpiration (λE_T) during wet and dry seasons with canopy and environmental controls over two different sites with different annual rainfall (2329 mm and 1597 mm, respectively) in the Amazon Basin (LBA tower sites K34 and FNS).

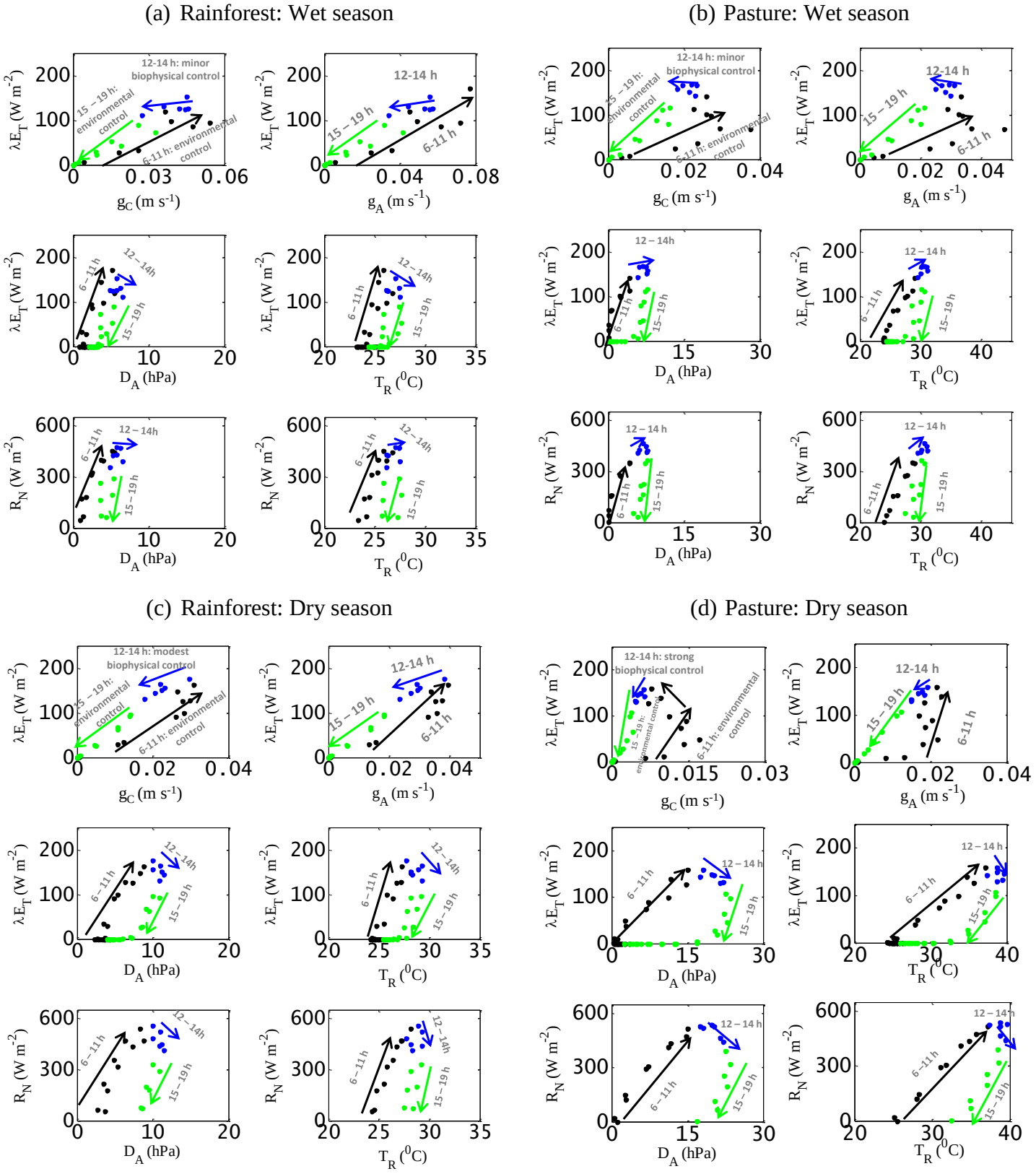

Figure 8. (a) Response of retrieved g_C to atmospheric vapor pressure deficit (D_A) for different classes of net radiation (R_N), (b) Response of retrieved g_C to transpiration for different classes of D_A, (c) Response of retrieved g_C to radiometric surface temperature (T_R) for different classes D_A, (d) Relationship between retrieved g_A and radiometric surface temperature and air temperature difference (T_R - T_A) in the Amazon Basin (LBA tower sites).

(a) g_C versus D_A

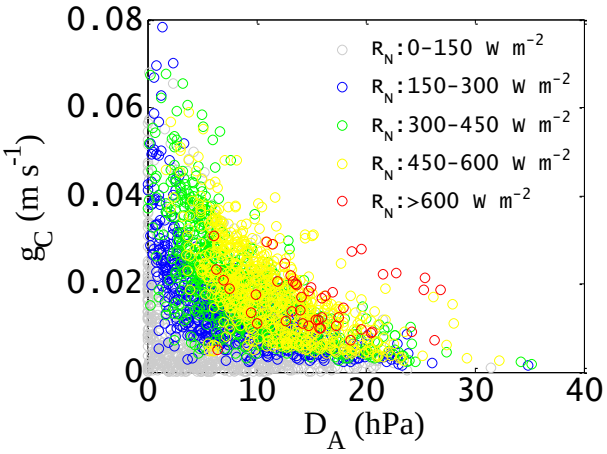

(b) g_C versus λE_T

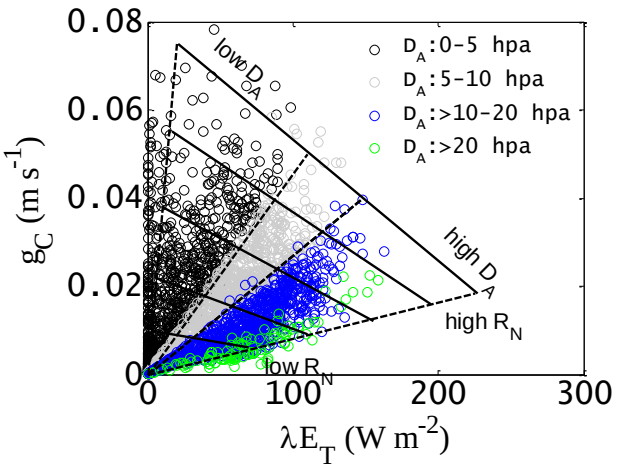

(c) g_C versus T_R

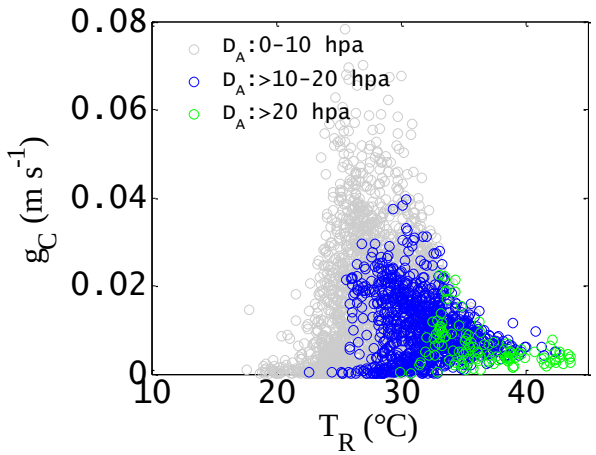

(d) g_A versus $T_R - T_A$

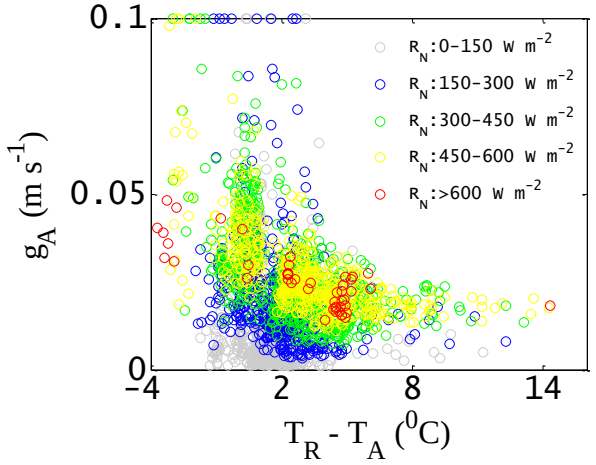

Figure 9. (a) Scatter plots between source/sink height (or in-canopy) vapor pressure deficit (D_0) and atmospheric vapor pressure deficit (D_A) for two different classes of g_C/g_A ratios over four PFTs, which clearly depicts a strong coupling between D_0 and D_A for low g_C/g_A ratios. (b) Histogram distribution of g_C/g_A ratios over the four PFTs in the Amazon Basin (LBA tower sites). (c) Scatter plots between g_C/g_A ratio versus surface air temperature difference (T_R - T_A) for the four PFT during wet season and dry season in the Amazon Basin (LBA tower sites).

(a) D_0 vs. D_A over four PFTs

(b) Distribution of g_C/g_A ratio over four PFTs

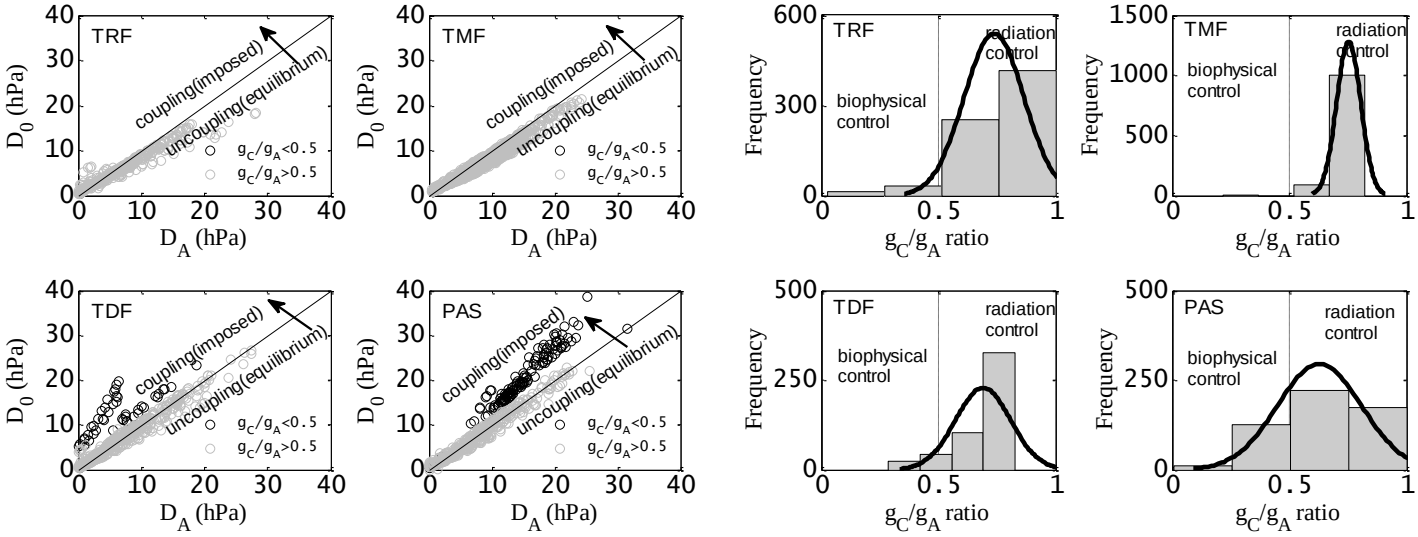

(c) g_C/g_A vs. T_R-T_A over four PFTs

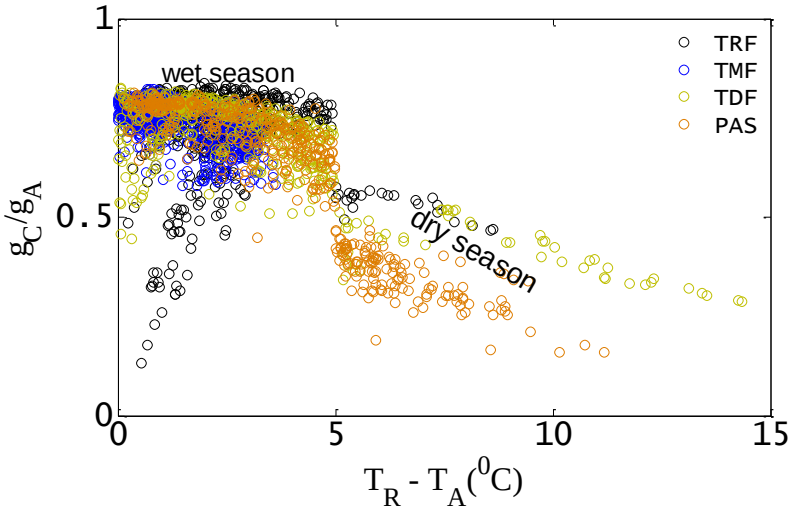

Table A1: Differences in the modeling philosophy of source/sink height vapor pressures (e_0, e_0^*) and dewpoint temperature (T_{SD}), surface wetness (M), and α between STIC1.0, STIC1.1 and STIC1.2.

Variable estimation	**Principles**		
	STIC1.0 (Mallick et al., 2014)	**STIC1.1 (Mallick et al., 2015)**	**STIC1.2 (This study [Mallick et al., 2016])**
Saturation vapor pressure at source/sink height (e_0^*)	e_0^* was approximated as the saturation vapor pressure at T_R.	Same as STIC1.0	e_0^* is estimated through numerical iteration by inverting the aerodynamic equation of λE (as described in appendix A2). $$e_0^* = e_A + \left[\frac{\gamma\lambda E(g_A + g_C)}{\rho c_P g_A g_C}\right]$$
Actual vapor pressure at source/sink height (e_0)	e_0 was empirically estimated from M based on the assumption that the vapor pressure at the source/sink height ranges between extreme wet–dry surface conditions.	Same as STIC1.0	e_0 is estimated as $e_0 = e_0^* - D_0$, where D_0 was iteratively estimated by combining PM with Shuttleworth-Wallace approximation (as described in appendix A2). $$D_0 = D_A + \left[\frac{\{s\phi - (s+\gamma)\lambda E\}}{\rho c_P g_A}\right]$$
Dewpoint temperature at source/sink height (T_{SD})	$T_{SD} = \frac{(e_S^* - e_A) - s_3 T_R + s_1 T_D}{(s_1 - s_3)}$ s_1 and s_3 are the slopes of saturation vapor pressures at temperatures, approximated at T_D and T_R, respectively.	Same as STIC1.0	T_{SD} is estimated through numerical iteration by inverting the aerodynamic equation of λE (as described in appendix A2). $$T_{SD} = T_D + \frac{\gamma\lambda E}{\rho c_P g_A s_1}$$
Surface moisture availability (M)	As a stand-alone equation, without any feedback to λE.	Same as STIC1.0	A feedback of M into λE is introduced and M is iteratively estimated after estimating T_{SD} (as described in appendix A2).
Priestley-Taylor parameter (α)	As fixed parameter (1.26).	A physical equation of α is derived as a function of the conductances and α is numerically estimated as a variable.	A physical equation of α is derived as a function of the conductances and α is numerically estimated as a variable (eqn. A15) (as described in appendix A2).

Table A2: Fundamental differences in the modeling principles between STIC1.2 and previous approaches for characterising the biophysical controls on λE components.

Biophysical states	**Modeling principles**	
	Parametric modeling (Ma et al., 2015; Chen et al., 2011; Kumagai et al., 2004)	STIC1.2
g_A	Either g_A is assumed to be the momentum conductance (g_M) or estimated as a sum of g_M and quasilaminar boundary-layer conductance (g_B). $1/g_A = 1/g_M + 1/g_B$ $g_M = u^*/u$ g_B = *f{Nusselt number, leaf dimension, thermal conductivity of air in boundary layer, u, kinematic viscosity, Reynolds number}* If u^* is available from EC tower, it is directly used, otherwise u^* is parametrized using Monin-Obukhov Similarity Theory (MOST). Disadvantages: (1) MOST is only valid for an extended, uniform, and flat surface (Foken, 2006). MOST tends to fail over rough surfaces due to breakdown of the similarity relationships for heat and water vapor transfer in the roughness sub-layer, which results in an underestimation of the 'true' g_A by a factor 1-3 (Thom et al., 1975; Chen and Schwerdtfeger, 1988; Simpson et al., 1998; Holwerda et al., 2012). (2) In the state-of-art λE modeling, the parametric g_A sub-models are stand alone and empirical, and do not provide any feedback to g_C, aerodynamic temperature (T_0), and aerodynamic vapor pressures (e_0 and D_0). (3) Additional challenges in grid-scale or spatial-scale g_A estimation are the requirements of numerous site specific parameters (e.g., vegetation height, measurement height, vegetation roughness, leaf size, soil roughness) and coefficients needed to correct the atmospheric stability conditions (Raupach, 1998).	Analytically retrieved by solving 'n' state equations and 'n' unknowns, with explicit convective feedback and without any wind speed (u) information. In a hallmark paper by Choudhury and Monteith (1986), it is clearly stated that 'aerodynamic conductance determined by wind speed and roughness is assumed to be unaffected by buoyancy. Strictly, the aerodynamic conductance should be replaced by a term which accounts for radiative as well as convective heat transfer'. The role of g_A is associated with the role of convection (Choudhury and Monteith, 1986) according to the surface energy balance principle as reflected in the derivation of eqn. (A4). Wind is generated as a result of the differences in atmospheric pressure which is a result of uneven surface radiative heating. Therefore, the aerodynamic conductance (and wind as well) is an effect of net radiative heating and there should be a physical relationship between these two. Advantages: (1) STIC1.2 consists of a feedback describing the relationship between T_R and λE, coupled with canopy-atmosphere components relating λE to T_0 and e_0. (2) Supports the findings of Villani et al. (2003) which stated that during unstable surface layer conditions the major source of net available energy is located at the canopy top and drives the convective motion in the layers above.
g_C	(a) If λE measurements are available from the EC towers, g_C is estimated by inverting the PM equation. None of these approaches allow independent quantification of biophysical controls of λE as g_C is constrained by λE itself. (b) Sometimes g_C is modelled either by coupled leaf-scale photosynthesis models (Ball et al., 1987; Leuning, 1995) or g_C is estimated from standalone empirical models (Jarvis, 1976)	Analytically retrieved by solving 'n' state equations and 'n' unknowns where physical feedbacks of g_A, soil moisture, and vapor pressure deficit are embedded (as explained in STIC1.2 equations in Appendix).

Figure A1. Schematic representation of one-dimensional description of STIC1.2. In STIC1.2, a feedback is established between the surface layer evaporative fluxes and source/sink height mixing and coupling, and the connection is shown in dotted arrows between e_0, e_0^*, g_A, g_C, and λE. Here, r_A and r_C are the aerodynamic and canopy (or surface in case of partial vegetation cover) resistances, g_A and g_C are the aerodynamic and canopy conductances (reciprocal of resistances), e_S^* is the saturation vapor pressure of the surface, e_0^* is the saturation vapor pressure at the source/sink height, T_0 is the source/sink height temperature (i.e. aerodynamic temperature) that is responsible for transferring the sensible heat (H), e_0 is the source/sink height vapor pressure, e_S is the vapor pressure at the surface, z_0 is the roughness length, T_R is the radiometric surface temperature, T_{SD} is the source/sink height dewpoint temperature, M is the surface moisture availability or evaporation coefficient, R_N and G are net radiation and ground heat flux, T_A, e_A, and D_A are temperature, vapor pressure, and vapor pressure deficit at the reference height (z_R), λE is the latent heat flux, H is the sensible heat flux, respectively.

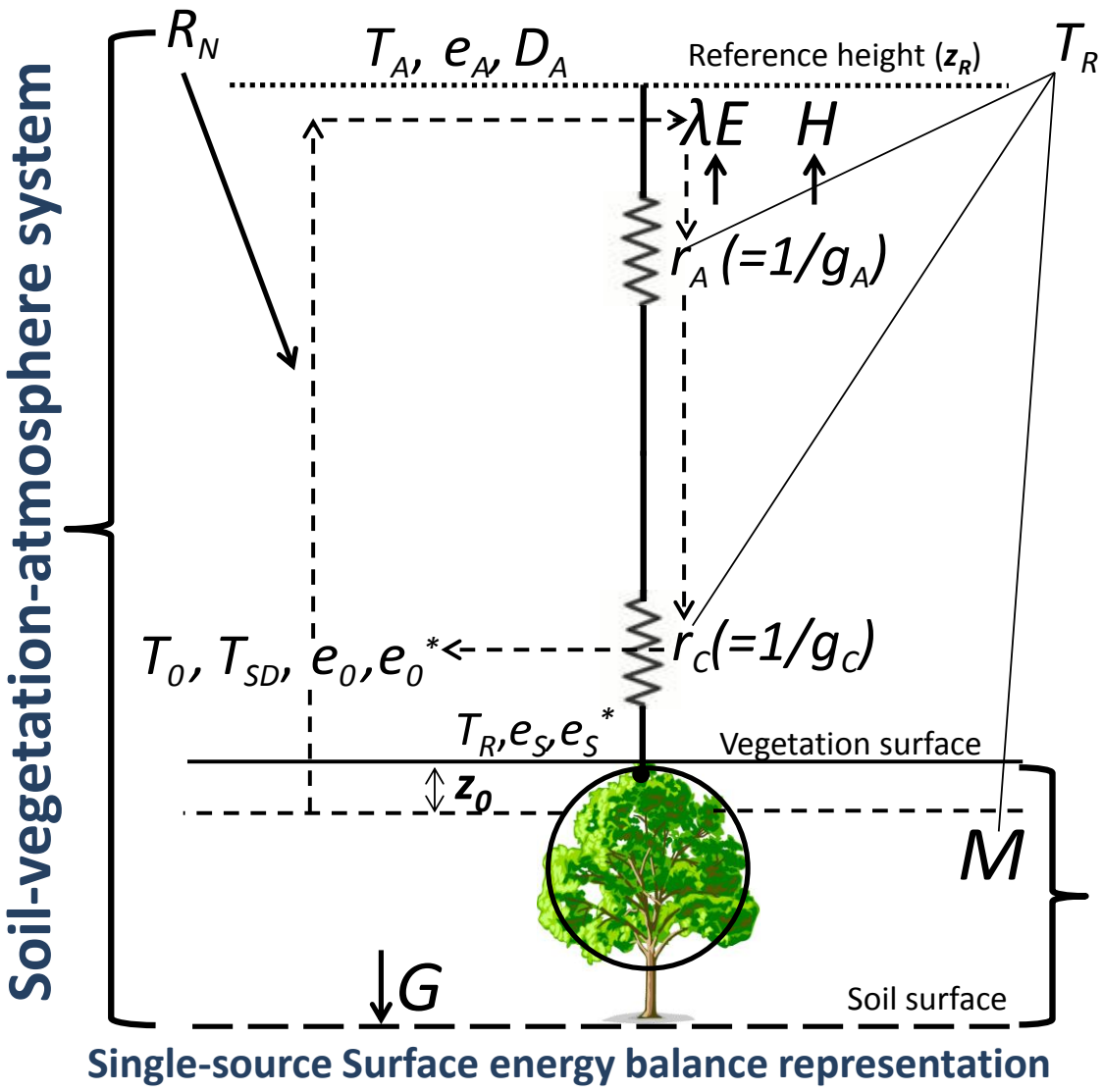

Figure A2. Aerodynamic temperature obtained from STIC1.2 ($T_{0\text{-}STIC}$) versus radiometric surface temperature (T_R) over two different biomes in the Amazon basin. The regression equation of line of best fit is $T_{0\text{-}STIC} = 0.67(\pm0.10)T_R + 10.59\ (\pm2.79)$ with $r = 0.65$.

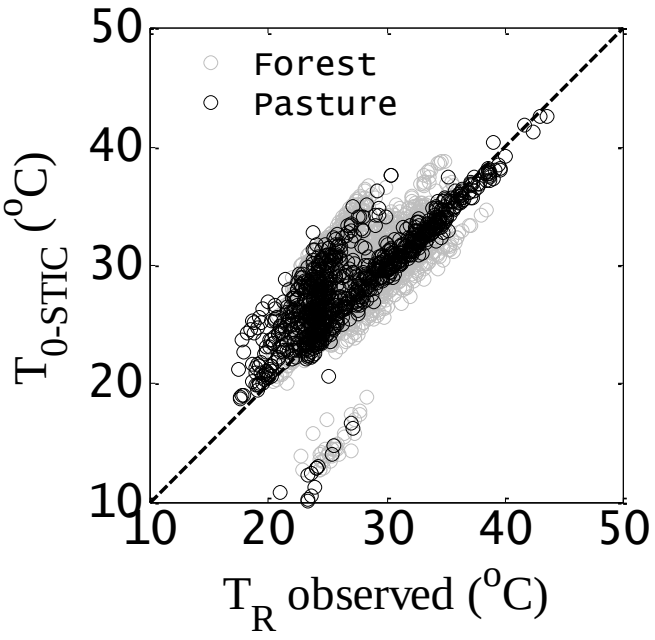

Figure A3. (a) Convergence of the iteration method for retrieving the source/sink height (or in-canopy) vapor pressures (e_0 and D_0) and Priestley-Taylor coefficient (α). (b) Convergence of the iteration method for retrieving the surface wetness (M) and source/sink height dewpoint temperature (T_{SD}). The initial values of λE, g_A, g_C, and T_0 were determined with α = 1.26. The process is then iterated by updating λE, e_0, D_0, M, T_{SD}, and α in subsequent iterations with the previous estimates of g_A, g_C, and T_0.